6 DISCUSSION

The geophysical data collected in the study area that have been used to construct the density model mostly fit. However, in some cases certain discrepancies exist. These, together with uncertainties associated with both lack of additional information and ambiguity of the forward density modelling technique, are discussed below.

6.1 Comparison to the constraining data

6.1.1 Comparison to the SPOC and ISSA profiles

Four cross-sections along the E-W seismic profiles are shown in Figures 6.1 and 6.2. They show the main structures derived from each of the geophysical methods, namely: combined wide-angle reflection/refraction seismic, local earthquake tomography and gravity results for the SPOC north, middle and south profiles and the ISSA profiles together with the receiver function. Where the wide-angle reflection / refraction seismic experiment or the receiver functions provide control on the continental Moho below the SPOC north and ISSA profiles, the Moho depths derived by the two seismic methods and gravity all agree, except at one place (marked by an ellipse in Figure 6.2) along the ISSA profile. Along the SPOC middle and south profiles where the wide-angle reflection/refraction seismic experiment essentially provides no control on the location of continental Moho, the Moho depths derived by gravity rise to levels where velocities of no greater than 7.0 km/s are reached.

A. SPOC north at ~36.15°S

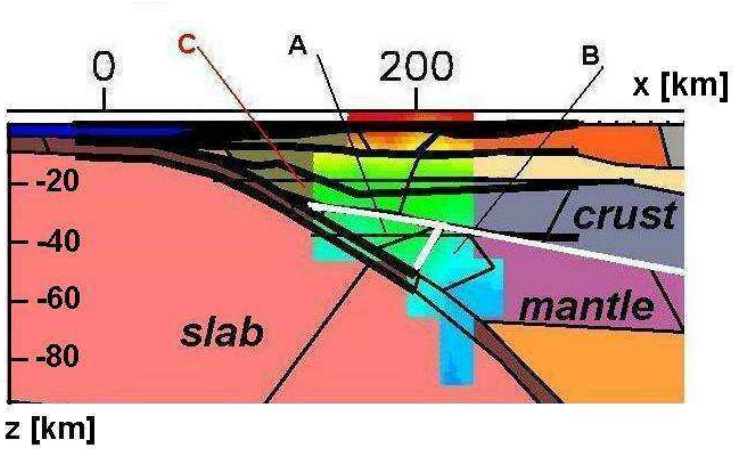

B. SPOC midlle at ~37.15°S

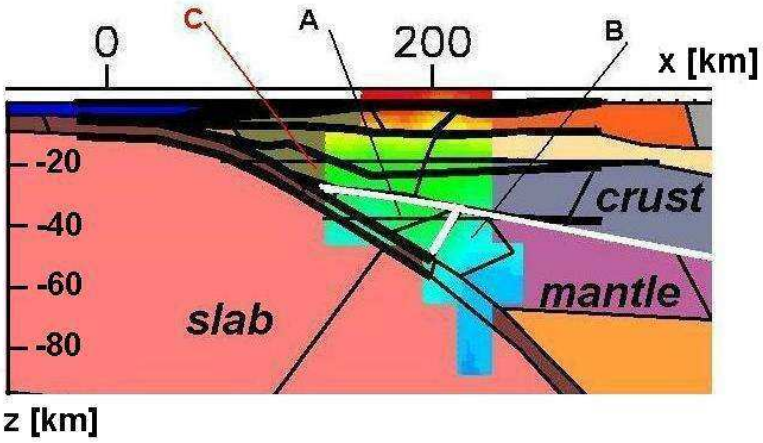

C. SPOC south at ~38.15°S

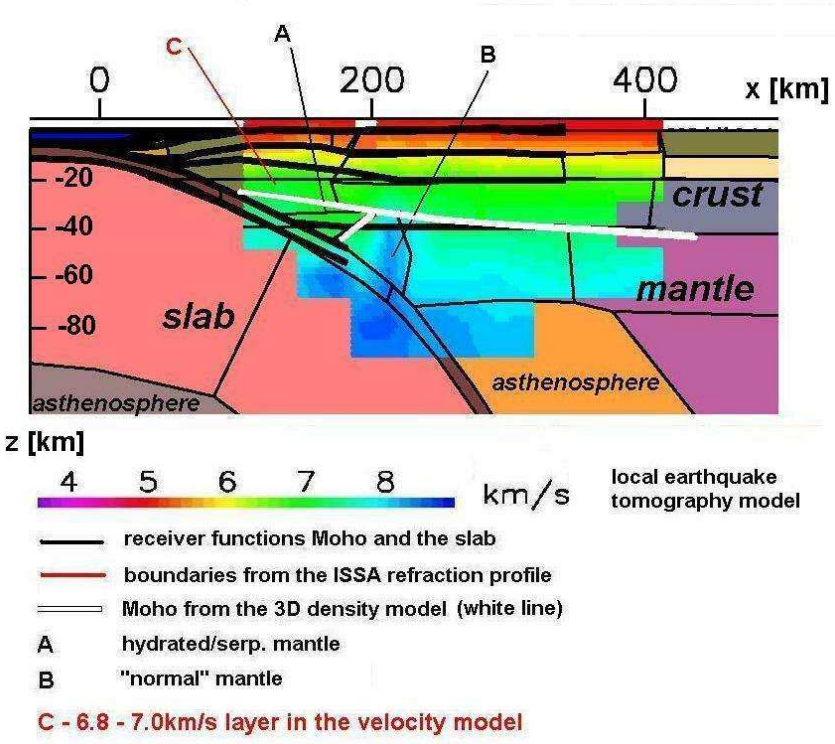

D. SPOC south steep-angle reflection seismic profile at ~38.15°S

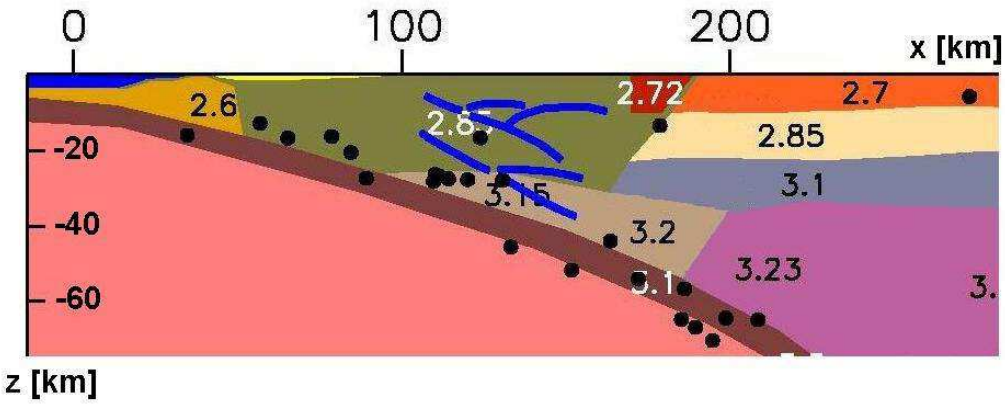

Figure 6.1 (above and opposite)
The structures of the density model together with the constraining data from the local earthquake tomography model and the SPOC velocity models. The upper boundary of the unidentified body at the bottom of the accretionary wedge (see Section 6.1.3) coincides with the observed Moho along the SPOC north profile (A), whereas along the middle (B) and south (C) profiles, to obtain a good fit to the observed gravity data, the Moho must lie within the 7.0 km/s velocity zone. The results of the reflection seismics along the SPOC south profile, which revealed detailed structures within the accretionary wedge (D, blue lines) correlate with the position of the upper boundary of the unidentified body.

The misfit exists along the ISSA profile below the Longitudinal Valley. The Moho boundary from the receiver function study does not agree with that derived from the local earthquake tomography, 2D refraction seismic, and the density models (Figure 6.2). The Moho imaged from the receiver function data shows a sharp shallowing, to depth of ~20 km below the coast. The density model, however, in which the crust/mantle interface is constrained by other data (local earthquake tomography and refraction), shows a more gradual shallowing and is some 12 km deeper.

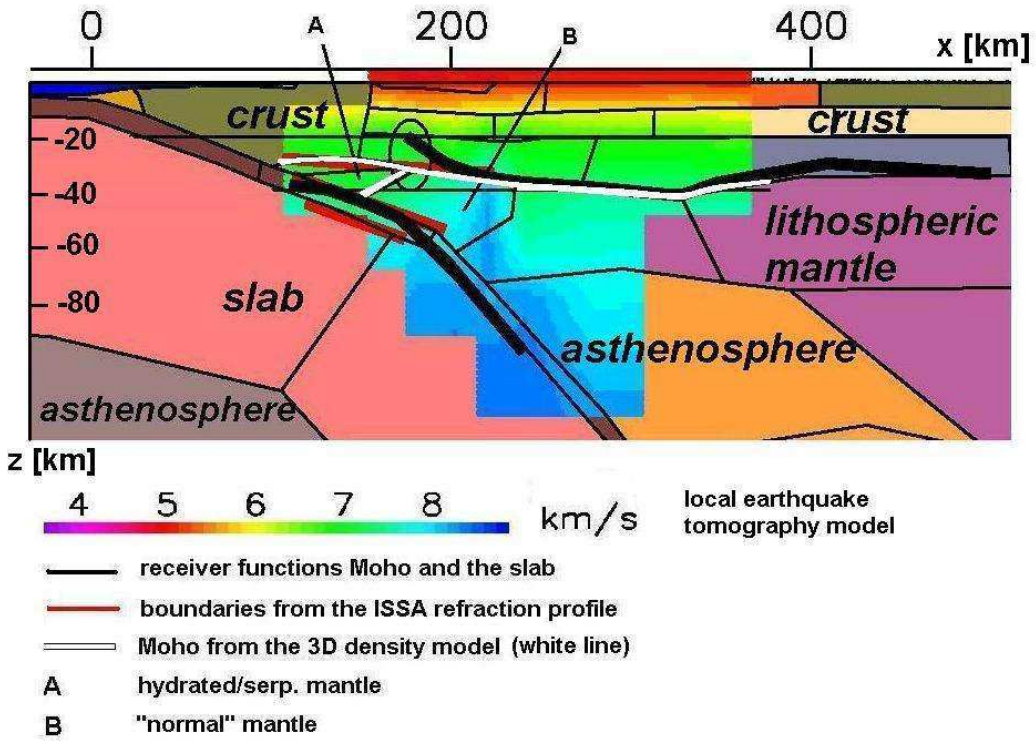

Figure 6.2
The fit of the density and velocity (refraction seismic and the local earthquake tomography) models, and misfit with the receiver function crust/mantle interface (thick black line). The difference in geometry is marked by the ellipse, where the density model Moho (white line) follows the refraction velocity profile (red) and deviates from the receiver function Moho by 12 km.

6.1.2 Comparison to magnetotelluric profiles

The magnetotelluric (MT) study (Brasse & Soyer, 2001; Section 4.2.2) along the ISSA profile revealed three conductors within the crust (Figure 4.7). These MT anomalies are displayed in Figure 6.3 as an overlay on the density model together with the Moho from the receiver function study and the lines from the ISSA refraction profile.

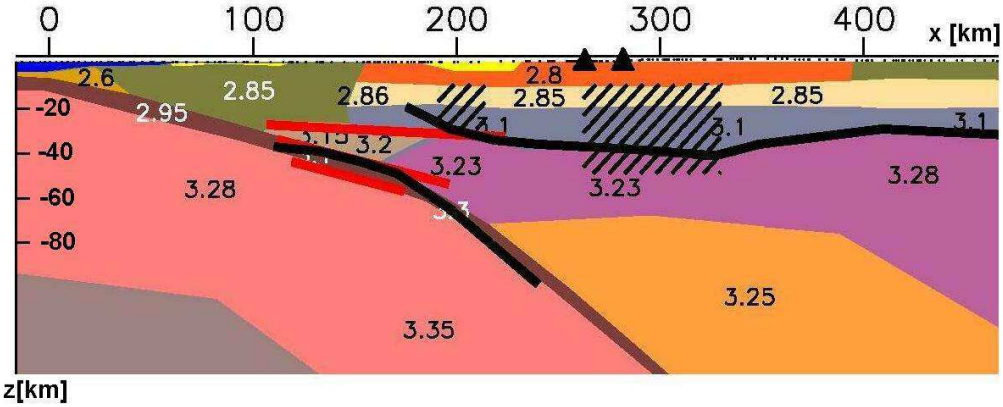

Figure 6.3

The low resistivity MT anomalies B and B' from Figure 4.7 are joined together into one rectangle in the middle (beige) and lower crust (gray layer), and the uppermost lithospheric mantle (lilac), below the volcanic arc (black triangles). This anomaly beneath the volcanic arc seems to be related to the major Liquiñe-Ofqui Fault Zone (LOFZ) that influences the distribution of volcanic activity along the volcanic arc. A good conductor (anomaly A in Figure 4.7), situated beneath the Longitudinal Valley (yellow), is also shown and thought to be related to the Lahnaluhe Fault Zone.

The central part of the low resistivity anomaly from the southernmost MT profile at ~39.3°S, is situated in the lower crust beneath the volcanic arc (Figure 6.4), but this anomaly is explained by Brasse and Soyer (2001) as an upper-mantle high conductivity zone (Section 4.2.2).

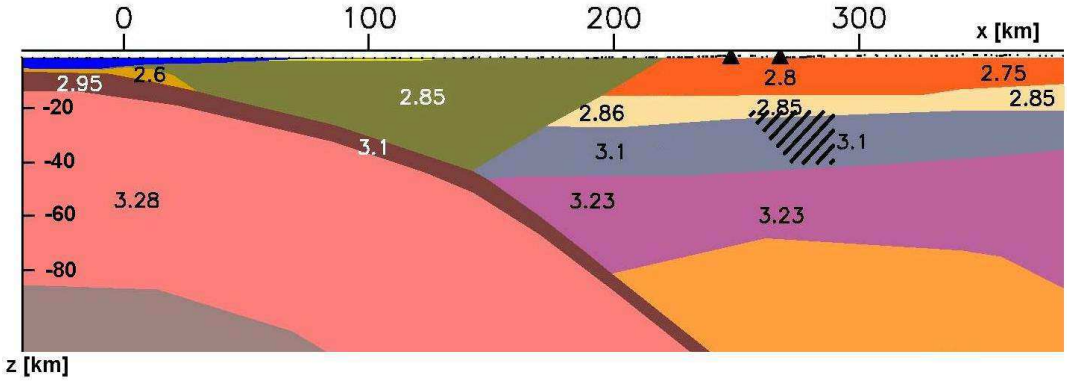

Figure 6.4

The low resistivity anomaly within the lower crust (gray layer) beneath the volcanic arc along the southern MT profile.

Because of the constant density values in the density model, none of the MT anomalies could be recognized in terms of anomalous gravity field, nor as density inhomogeneities within the middle and lower crustal layers. A very good conductor below the Longitudinal Valley along the ISSA profile (Figure 6.3) partly coincides with the misfit between the receiver function Moho (Figure 6.2), and the Moho inferred from other data. However, it is unrelated to the previously discussed unidentified body.

6.1.3 Comparison to the local earthquake tomography model

Another point of the discussion is the structure of the forearc crust and the depth of the uppermost mantle. One interpretation is based on the local earthquake tomography model by Bohm et al. (2003) (Figure 4.3). In this model the crust is thinner below the Longitudinal Valley, whereas below the volcanic arc the crust thickens to ~50 km. Also, velocities of the uppermost lithospheric mantle below the Longitudinal Valley are higher than beneath the volcanic arc. A smaller part of the uppermost mantle below the Coastal Cordillera corresponds to a low velocity zone in the tomography model and is interpreted to be serpentinized mantle (Bohm et al., 2003).

Forearc lithospheric mantle

The shallower mantle beneath the Longitudinal Valley is a part of the forearc lithospheric mantle, and lies directly above the asthenospheric mantle wedge. There the convecting asthenospheric mantle material interacts with the fluids and melts derived from the subducting slab, and arc magmas are generated (van Keken, 2003). The lithospheric mantle directly above it is, according to some observations, hydrated and/or serpentinized (e.g. Stern, 2002). In this case, density values are lower than normal mantle densities, despite the forearc temperatures being lower than those below the volcanic arc. The forearc mantle is expected to be cooler, because of the cooling effect from the relatively cold incoming slab, whereas the lithospheric mantle below the volcanic arc is thought to be hotter due to melt transport. Because of these two factors (hydration in the forearc and heat below the arc), and the simplicity of the modelled structures, the density values of both parts of the mantle within the 3D density model are the same (3.23 Mg/m^3), whereas the forearc mantle in the tomography model is imaged as a velocity zone with higher velocities than those below the arc at the same depths (further discussion in 7.3).

However, the density modelling generally supports the interpretation of a high velocity zone, because a density of 3.23 suggests a low degree of hydration/serpentinization. As shown in Figure 6.5, if the uppermost part of the mantle was modelled with density values of 2.9 and 3.0 Mg/m^3, typical for 30% to 40% serpentinization, the response in the calculated gravity field is enormous.

6.5. A.

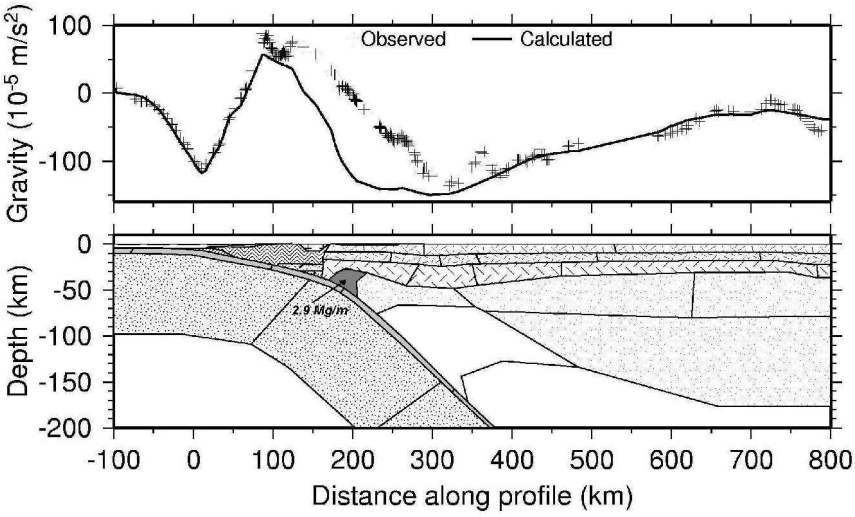

6.5.B.

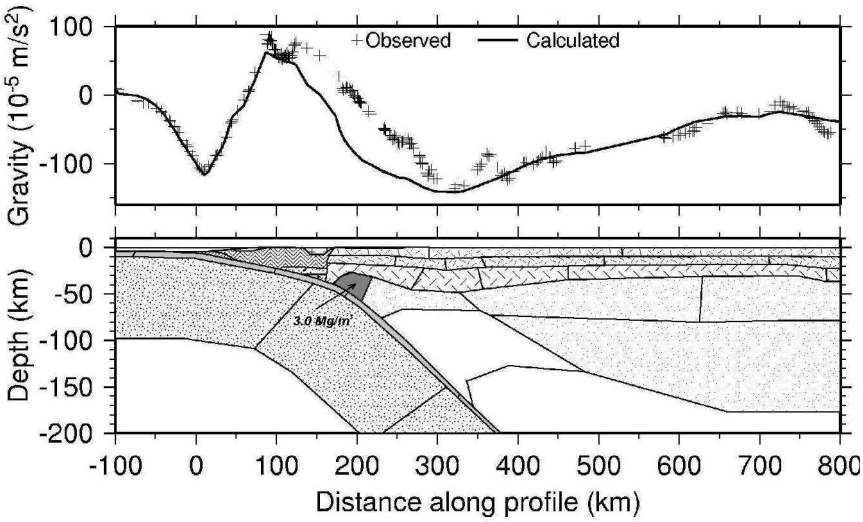

Figure 6.5

The effect of lower density forearc lithospheric mantle. Densities of 2.9 (A) and 3.0 Mg/m^3 (B), corresponding to 30 to 40% serpentinized mantle were tested and found to be too low to reproduce the measured gravity. The large mass deficit in the modelled gravity field could be reproduced only by an extremely dense crust and slab (see legend, C).

6.5.C

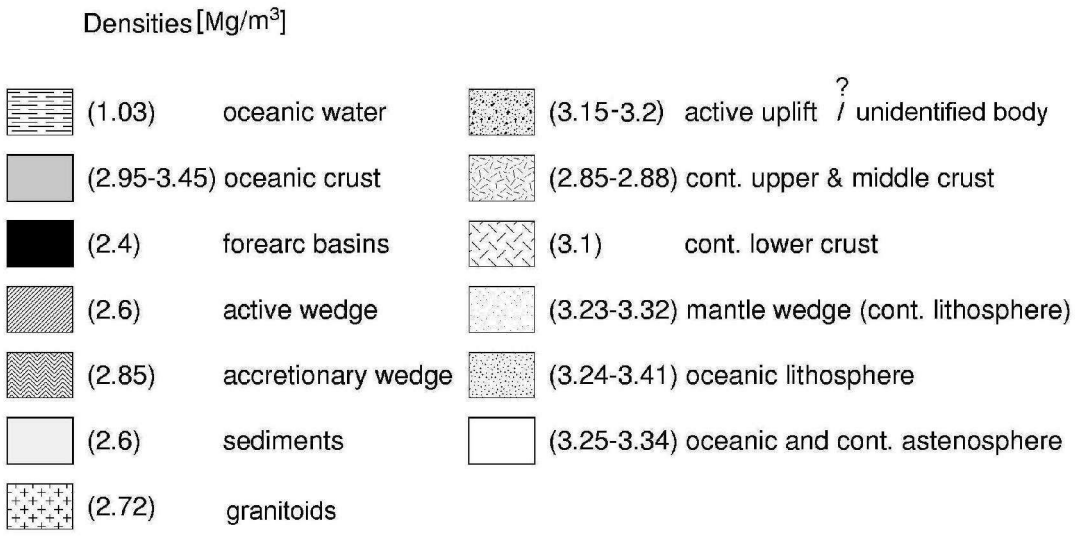

Figure 6.5 continued

Therefore, these examples support the interpretation of high velocity structure within the mantle, which requires higher densities than the values estimated for a slow, serpentinized/hydrated mantle. If all the densities (also within the slab) have been modelled correctly, then the density value of 3.23 Mg/m^3 suggests that 10% serpentinized mantle is present within the forearc lithospheric mantle (Hacker et al. 2003).

Forearc serpentinized lithospheric mantle

Uncertainty surrounds a small structure (unidentified body, Figure 6.1) in the forearc located in between the slab and the shallow mantle below the Longitudinal Valley (Figures 6.6 and 6.7, black ellipse). In the local earthquake tomography model, this body has P-wave velocities of 6.5 – 7.5 km/s at depths of 30–50 km. This structure has been interpreted from the local earthquake tomography to be serpentinized mantle. In the density model, however, this body was initially modelled as basally accreted material, thought to be responsible for the positive Bouguer anomaly and uplift in the Arauco-Lonquimay segment. Whilst the mass of this body has an important influence (at short wavelengths) on the gravity high, as

will be shown in following section (6.3.3), this feature is not solely responsible for the positive anomaly. In order to fit the observed gravity values, the density of this body must be 3.15 to 3.20 Mg/m^3 and its length and thickness some 50 km and 15 km, respectively. Therefore, the high densities inferred from the density model mean that it is difficult to interpret this body as subducted sediments only.

In the initial density model, this body was situated oceanward of the region of serpentinized mantle imaged in the local earthquake tomography model. The black ellipse in Figure 6.6 shows the “problematic spot”. The area of slow velocity (~7.0 km/s) seen in the local earthquake tomography model was previously modelled in the density model partly as normal mantle and partly as a lower crust with a density of 3.1 Mg/m^3, which could also explain the slow velocity.

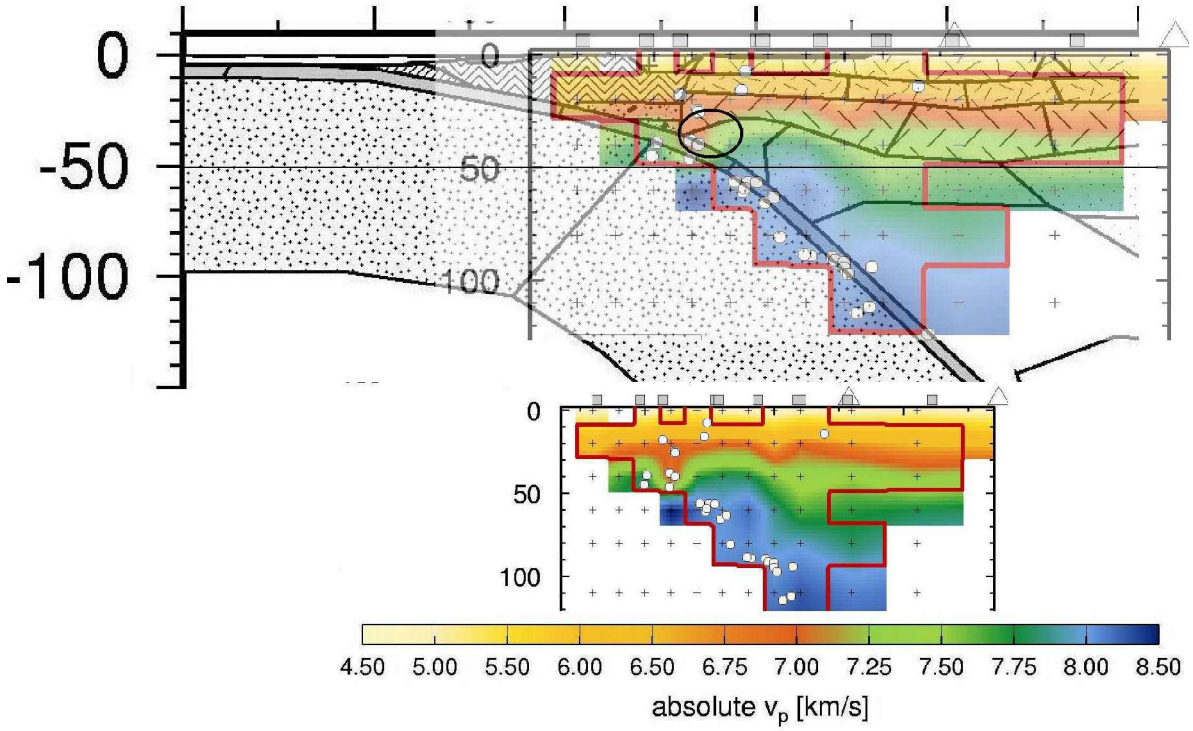

Figure 6.6
The local earthquake tomography model model (Bohm et al. 2003, Bohm, 2004) approximately overlain on the initial density model demonstrates the difference in structure between the interpretation based on the local earthquake tomography model and the preferred density model. The velocity values are shown below the overlay. The red box marks the area where local earthquake tomography model was resolved. The black ellipse in the overlay image denotes the “problematic spot”, where the difference occurs.

If the body is shifted eastwards such as it becomes part of the normal mantle (Figure 6.7), it replaces the original normal mantle material and the lower crust in the density model. Changing the forearc geometries in this way does not have any major impact on the modelled gravity values.

This part of the forearc was also imaged in the results of the SPOC and ISSA wide angle reflection / refraction seismic profiles, and was interpreted as hydrated mantle because of a very smooth transition from slow to high mantle velocities (Lüth et al., 2003). The observed P-wave velocities from the SPOC and ISSA profiles range from 7.2 to 7.3 km/s at the observed and/or assumed point of intersection of the continental Moho with the slab at 30–40 km depth. The velocity values above this point are 7.0 km/s. The unidentified body in the density model lies between 20 and 50 km depth and according to the velocity-density conversion results (Table 4.2), the density of 3.15 Mg/m^3 at 20 km depth used in the density model would be too large a value for the observed velocities.

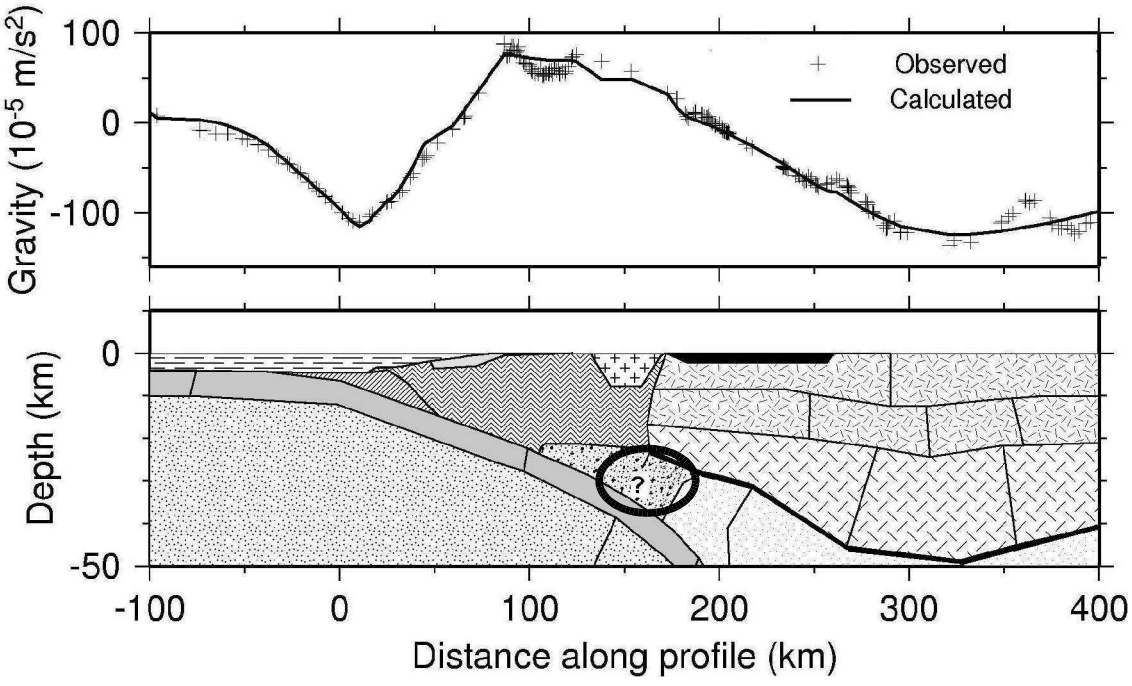

Figure 6.7

The forearc geometry modified according to the local earthquake tomography model. The lower crust (with the Moho marked by the thick black line; for other structures see legend in Figure 6.5.C) and part of the “normal” mantle has been replaced by the supposed serpentinized mantle (black ellipse). However, the size of this body required in the density model to fit the measured gravity values, is greater than it is interpreted from the local earthquake tomography model. As shown in Figures 6.1 (A,B,C) with velocity profiles overlain, the upper part of this structure in the density model lies within the 7.0 km/s velocity zone, imaged in the SPOC models as a part of the crust.

Based on Hacker et al. (2003), 100% serpentinized harzburgite would have a density of 2.6 Mg/m^3, whereas a normal harzburgite would have density of 3.30 Mg/m^3. Therefore a density of 3.15 Mg/m^3 could be explained by a mixture of 20% fully serpentinized mantle mixed with 80% normal mantle, whereas 10% fully serpentinized mantle with 90% normal mantle would give a density of 3.23 Mg/m^3. The P-wave velocity of 7.0 km/s however, could also correspond to ~30% serpentinized lherzolite, based on the estimation of the method of Hacker and Abers (2004). Such serpentinized mantle would have a density of 2.9 Mg/m^3. This value is much too low for the measured gravity (Figure 6.8) and would cause a mass deficit of ~40 .10^{-5} m/s^2.

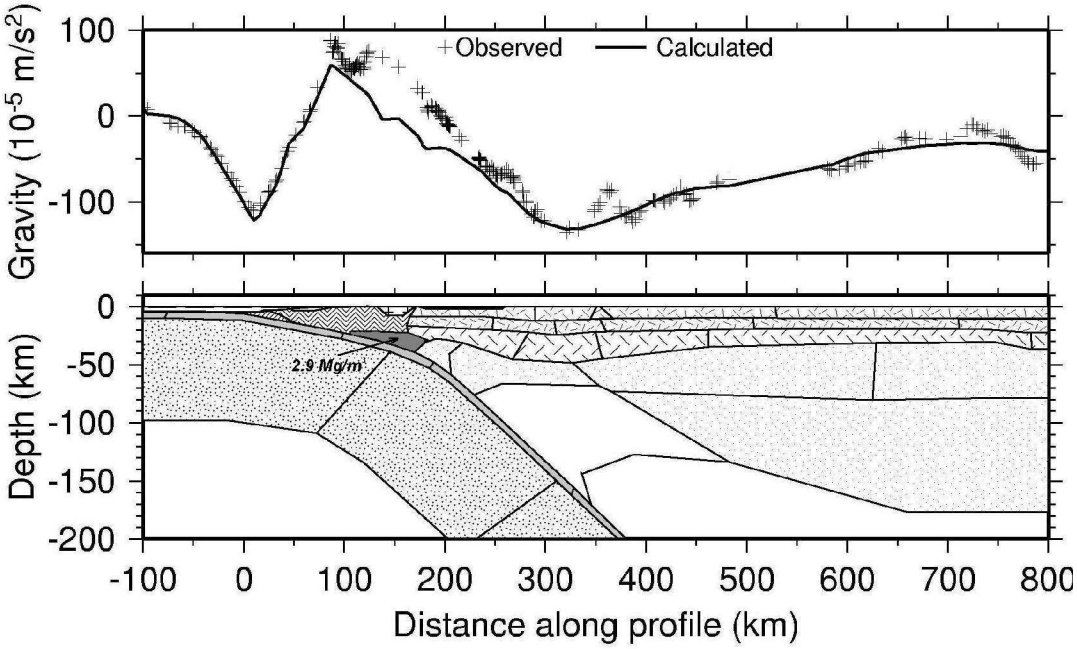

Figure 6.8
Low density values for the unidentified forearc body would cause a local collapse of the calculated gravity, exceeding the assumed accuracy of the measured Bouguer gravity anomaly.

6.1.4 Misfits between the gravity model & other geophysical data

The final density model has following misfits with other geophysical data:

1.) The crust/mantle interface beneath of the accretionary wedge

The unidentified body in the density model is modeled as having two layers and, in order to fit the observed gravity data, it is bigger than imaged in the local earthquake tomography model. The modeled densities have values of 3.15 and 3.2. These density values should be lower because the P-wave velocity values for

this body from the SPOC profiles are 7.0 to 7.2 km/s. The densities could be 3.1 and 3.15 Mg/m^3 for the upper and lower part, respectively. The density 3.1 Mg/m^3 would better correspond to the 7.0 km/s velocity at ~30 km depth. However, to match the observed gravity field, the mass deficit resulting from the lower density would have to be compensated by a denser underlying slab. Increasing the density of the oceanic crust to 3.15 Mg/m^3 (instead of the previous value of 3.1 Mg/m^3) would compensate the mass deficit of the unidentified body if it had an average density of ~3.15 Mg/m^3. If the unidentified body had a density of 3.1 Mg/m^3, the crust of the slab underlying the forearc would require a density of 3.2 Mg/m^3. The part of the slab that must be modified corresponds to blueschist-greenschist facies, which normally does not achieve such high densities at 30 km depths. However, with no constraints on thermal structure, it is impossible to determine slab density more accurately. Also, a denser slab would mean an increase in mass south of 39° S, where the unidentified body does not exist. This would require a slab position deeper than in the preferred model.

2.) The lithospheric mantle density

In the local earthquake tomography model beneath the Longitudinal Valley, the forearc lithospheric mantle has higher velocities than beneath the volcanic arc. Thus, a density change should also be observed. However, the lithospheric mantle in the density model has a constant density beneath the Longitudinal Valley and the volcanic arc. To be consistent with the local earthquake tomography model, higher density should be used in the mantle below the Longitudinal Valley. Due to the increased mass excess, this would increase the Moho depth. The asthenospheric mantle wedge was modelled with a density value of 3.25 Mg/m^3, as low S-wave velocities were observed in the wedge of the Central Andes by S. van der Lee et al. (2003) and high temperatures are expected there due to melt generation. Thus, the overlying lithospheric mantle should also not exceed this density. That means a density increase of no more than 0.02 Mg/m^3 for the lithospheric mantle beneath the Longitudinal Valley. This increase would cause the crust/mantle interface there to be deepened some 1 to 2 km.

3.) The crust/mantle interface

It should be also noted that the Moho in the density model does not always follow the 7.75 km/s isoline, which in the local earthquake tomography model marks the crust/mantle interface (Bohm, 2004). The Moho in the density model generally follows the structure of the local earthquake tomography, but is adjusted to the observed gravity field and other geophysical data. Using the results of the receiver function study imaging the Moho at 40 km depth along the ISSA profile, the depth of the Moho and the density value of the lower crust, were constrained. At this depth, below the volcanic arc, the P-wave velocity from the local earthquake tomography model reaches ~7.3 km/s. To model the crust/mantle interface at depths equivalent to 7.75 km/s, which from the local earthquake tomography model along the ISSA profile is even below 55 km, requires a large density increase within the crust. The same is true for most of the main arc, where the local earthquake tomography shows thicker crust than used in the density model, using a density value of 3.1 Mg/m^3 in the lower crust. Along the ISSA profile, however, the Moho from the density and receiver function models, fits well with the Moho from the local earthquake tomography model beneath the Longitudinal Valley. The P-wave velocity of 7.75 km/s is observed there at the depth of ~35 km. The crust/mantle interface in the density model also generally matches the Moho predicted from the local earthquake tomography model beneath the Longitudinal Valley in the rest of the model.

This indicates that either an across-strike density variation is necessary in order to maintain a Moho that matches the 7.75 km/s isoline below the volcanic arc (a minimum density value of 3.15 Mg/m^3 in the lower crust would be required below the main arc; Figure 6.14), or the crust/mantle interface in the local earthquake tomography model is too deep. Based on the data from geology and geochemistry, 50–55 km thick crust along the volcanic arc from 36 to 39°S, is not expected (Haschke, pers. comm., 2004). Therefore, the density of the lower crust in the density model is kept homogeneous (3.1 Mg/m^3). Hence, the Moho in the density model is observed at depths that correspond to P-wave velocity values of ~7.3 to 7.75 km/s in the local earthquake tomography model. To maintain simplicity, and because of a lack of additional constraining information, no across-strike density changes are incorporated in the gravity model.

Despite the above listed differences, the density model is generally in good agreement with the constraining geophysical data.

6.1.5 Euler deconvolution

The interpretation based on the forward density modelling (Section 6.5) was also tested independently by an Euler deconvolution method for detection of anomaly sources.

Euler deconvolution has been applied to magnetic and gravity data in geophysics for more than 30 years. It is based on Euler's homogeneity equation enunciated in the 18th century. Euler deconvolution can be used to help speed interpretation of any potential field data in terms of depth and geological structures. With this technique, the field and its three orthogonal gradients (two horizontal and the vertical) are used to compute anomaly source locations.

Euler deconvolution by means of regularization

The calculation of potential fields gradients (higher derivatives) is an unstable problem, which is being improved by regularization tools (Pašteka and Richter, 2002). The regularized derivatives that are used for the 3D Euler algorithm are based on the Tikhonov approach with enhancements by Pašteka (2000). This approach solves transformation indirectly as an optimization problem by minimizing two functionals, where the first one describes the proximity of the inverted solution to the original data and the second one describes the smoothness of the obtained solution. The calculation of derivatives is performed in the spectral domain by means of the Fast Fourier Transformation (FFT) multiplied by the regularization filter for one selected (optimal) regularization parameter (Pašteka and Richter, 2002). The result of the Euler deconvolution is the depth estimation of the Euler solutions (locations of anomaly sources) for a structural index 0, which in gravimetry means thin long bodies. Figure 6.9 shows Euler solutions for the study area computed by Pašteka (pers. comm. 2004).

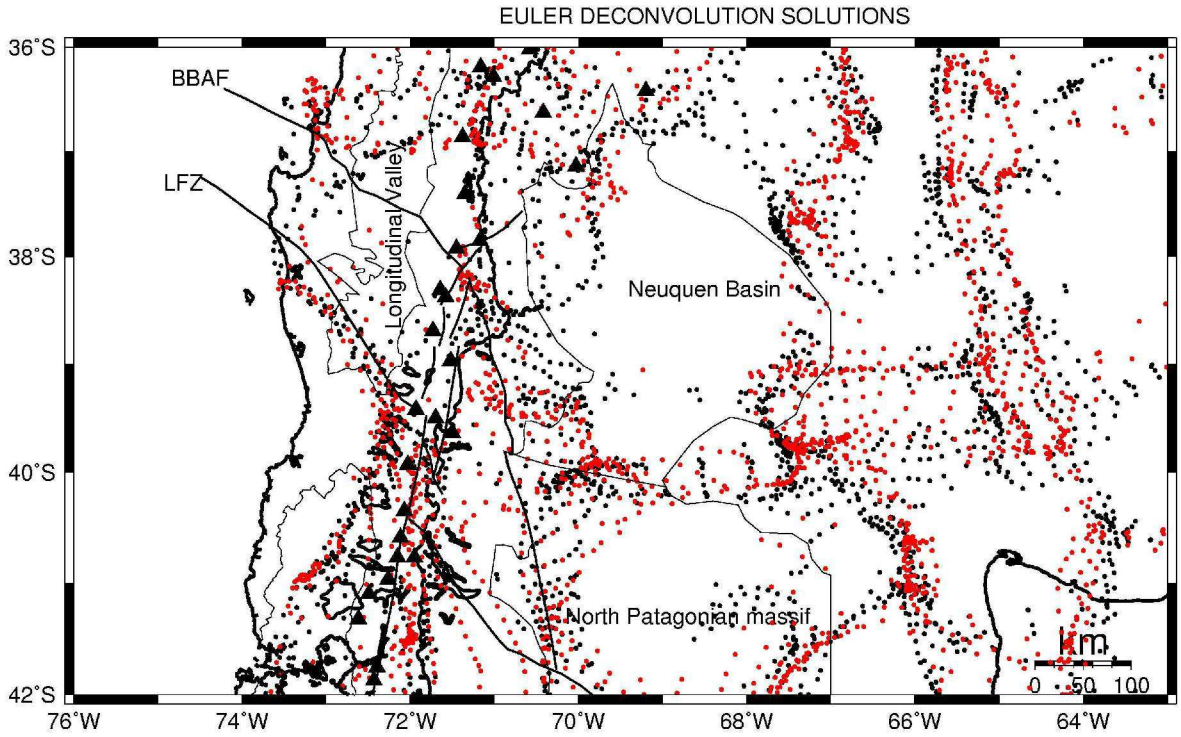

Figure 6.9
Euler solutions (source depths) derived for two different regularization parameters. One set of solutions show deeper results (depths between 0–90 km, red dots) than the other (0–60 km depth, black dots). The horizontal position of sources is, however, very similar for both parameters. Selected morphological units and major faults are overlain, and highlight correlations between surface structures and source depths. Many Euler solutions seem to be associated with the boundary of the Neuquen Basin and the North Patagonian massif in the backarc; in the forearc they seem to be concentrated along the Lahnaluhe Fault Zone (LFZ) and in the central part of the Longitudinal Valley south of 40°S. Correlation between the Euler depth solutions along the volcanic arc (black triangles) and the Bío-Bío-Aluminé Fault (BBAF) are less pronounced.

When the Euler deconvolution solutions are projected onto the cross-sections of the density model, some profiles in the Arauco-Lonquimay and Bahía Mansa-Osorno segments show a good correlation between source depths and the Moho where the crust is thinned below the Longitudinal Valley (Figures 6.10–6.12). In part there is also a correlation between the source depths and the part of the forearc of uncertain origin (Figure 6.10).

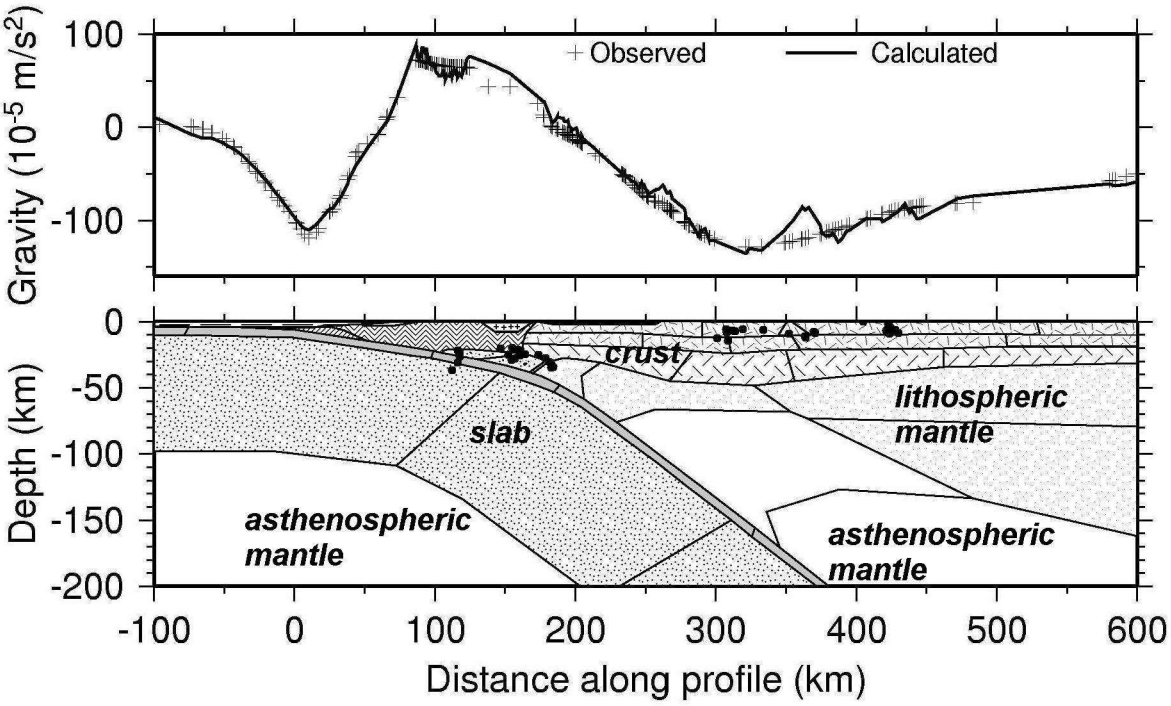

Figure 6.10
A cross section from the Arauco-Lonquimay segment at ~37.3°S where the Euler solutions fit well with the upper boundary of the high density body at the base of the accretionary prism (Section 6.1.3). The legend is shown in Figure 6.5.C.

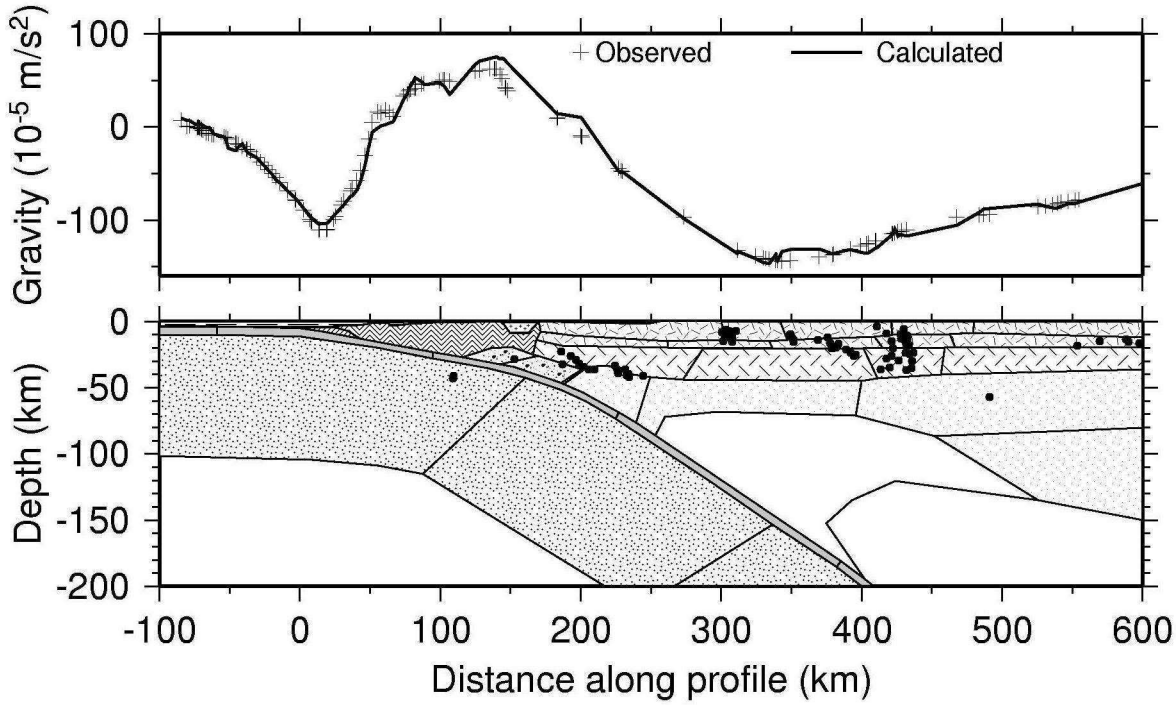

Figure 6.11
A cross section from the Arauco-Lonquimay segment at 37°S where the Euler solutions fit well with the crustal thinning associated with the Longitudinal Valley. The features represent the same structures as in the figure above; the legend is the same as in Figure 6.5.C.

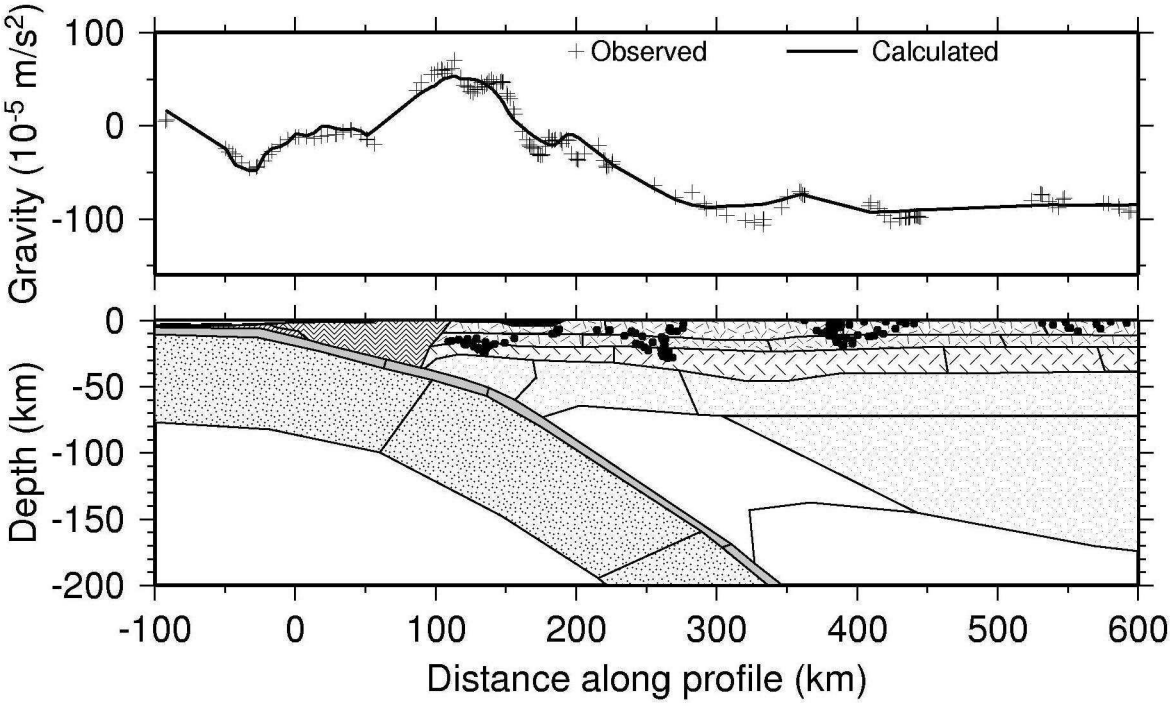

Figure 6.12
A cross section from the Bahía Mansa-Osorno segment at 40.8°S where the Euler solutions are situated within the middle and lower crust below the Longitudinal Valley. The fit with the crustal thinning is not as good as in the Arauco-Lonquimay segment (Figures 6.10 and 6.11), but the trend of the horizontal location of the anomaly sources, agrees.

In the Valdivia and Bahía Mansa-Osorno segments, the solutions occur within the crust and mark the boundaries between the upper, middle and the lower crustal layers, but do not reach the crust/mantle interface.

6.2 Varying parameters related to the continental crust

6.2.1 Modified lower crustal densities and thickness

Because forward density modelling is ambiguous, also other geometries and densities within the crust can also match the observed gravity data. To show these possibilities, as well as to quantify the dependence of the Moho depth on the assigned densities, the following tests were performed.

1.

First, the lower crust was assigned a lower density value of 3.0 Mg/m^3, corresponding to a felsic composition. The model requires a thin crust to compensate for the mass deficit caused by this low density. Such a model results

in an average crustal thickness of 35 km, with a minimum of 22 km below the Longitudinal Valley south of 40°S and a maximum of 42 km below the main arc at 36.5°S. The volcanic arc has an average crustal thickness of 30–34 km and the crust below the Longitudinal Valley is 23–30 km thick (Figure 6.13).

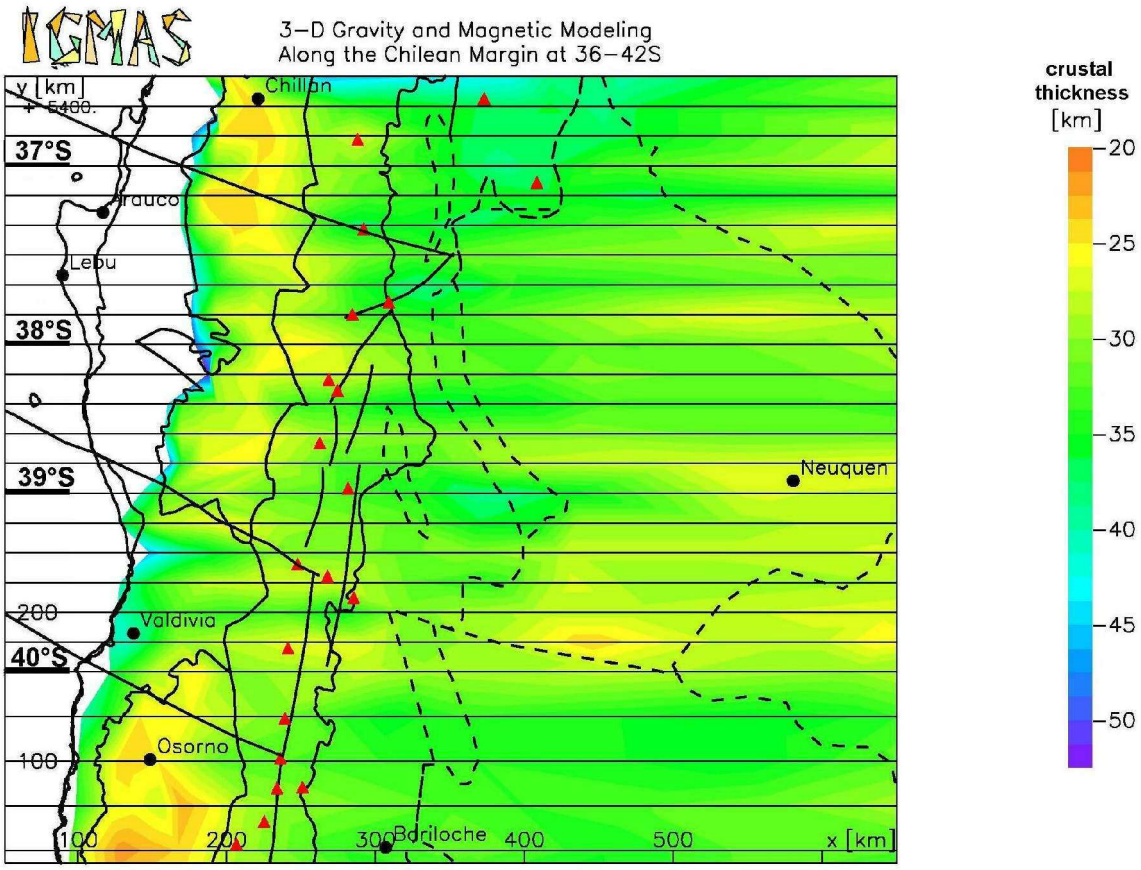

Figure 6.13

The changed crustal thickness caused by reducing the lower crustal density by -0.1 Mg/m^3 from the density of 3.1 Mg/m^3 of the lower crust in the preferred density model. Less dense crust has to be compensated by a decrease of 5–10 km in the crustal thickness. The three segments of the study area (black lines) are shown together with the morphological units and the volcanic arc (red triangles). (see Figures 5.16 and 2.5).

2.

Second, the lower crust was assigned a high mafic density of 3.15 Mg/m^3. The mass excess related to this change requires much thicker crust, reaching an average thickness of 50 km, a maximum thickness of 63 km at the volcanic arc (~36.5°S) and a minimum thickness of 33 km in the forearc (Figure 6.14). The volcanic arc is then characterized by an average crustal thickness of 48–55 km. The Longitudinal Valley south of 40°S has 33–42 km thick crust, whereas north of 39°S it increases by ~5 km.

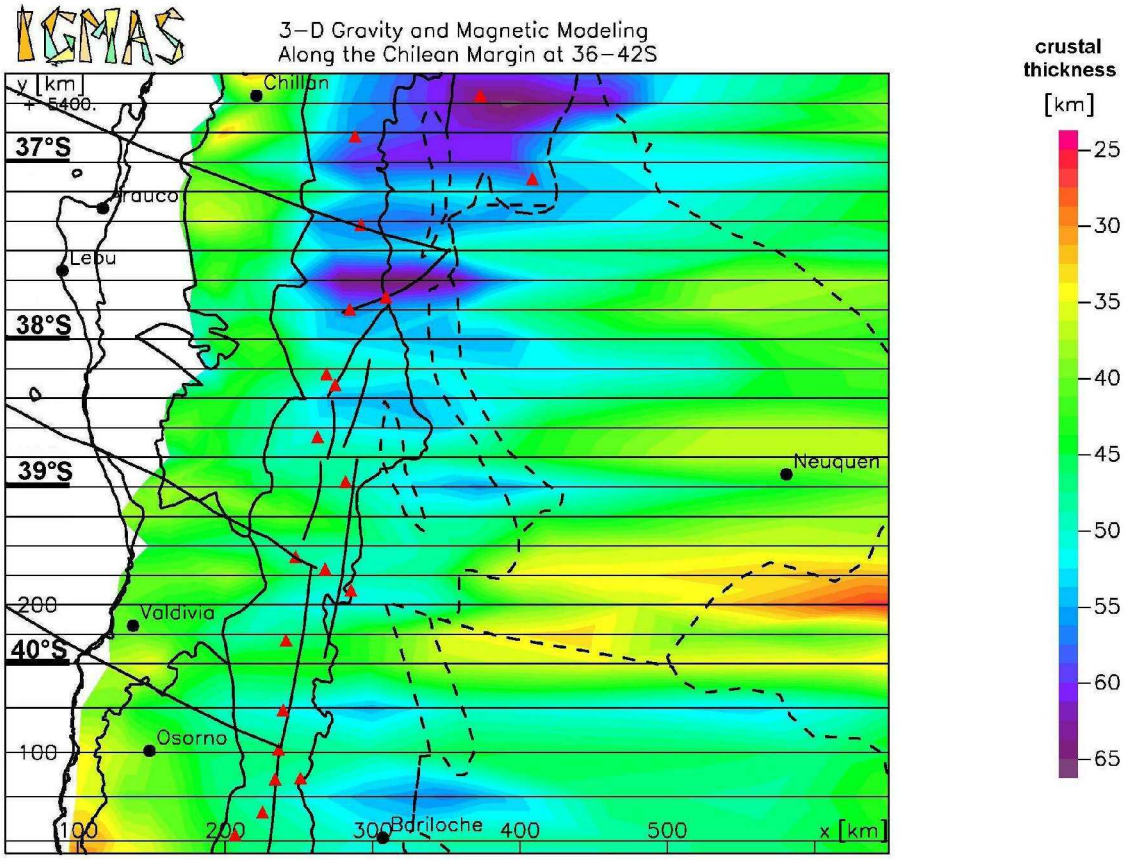

Figure 6.14

The changed crustal thickness related to a density difference of +0.05 Mg/m^3 from the original density value of 3.1 Mg/m^3 of the lower crust in the preferred model. A denser lower crust has to be compensated by 5–10 km greater crustal thickness. See Figure 6.13 for explanation of symbols.

This test shows that if a dense mafic lower crust could be proven to exist, for instance from petrological observations, the crust would be characterized by an average thickness of 50 km (assuming that the upper and middle crustal geometry and density are correct). On the other hand, if a thin crust is to be expected, the lower crustal composition will not achieve the density values of a mafic composition. Hence, under the assumption that the upper and middle crustal layers have been modelled correctly, the crust cannot be thin and mafic at the same time. If the crust was to be thin and the lower crust mafic, the upper and middle crustal layers would have to be less dense and/or thicker, to compensate the mass excess. This would have the following consequences:

1. The upper crust would remain the same as in the preferred model, but the middle crust would be less dense (2.75 Mg/m^3 instead of 2.85);

2. The upper crust would be less dense (2.6–2.75 Mg/m^3, depending on the area), and the middle crust would not change;
3. Both of them would have to be thicker and/or less dense than in the preferred model.

6.2.2 Conclusions for the continental crustal structure

In the previous section, three possible lower crustal models that can suitably explain the observed gravity field were described. The first alternative has a thin crust with a low density lower crust (Figure 6.13); the second has a mafic lower crust of high density, causing a thick crust (Figure 6.14), and the third could be a combination of both. A thin crust with high density in the lower crust, requires the upper and middle crustal layers to be less dense and/or thicker than those of the final density model described in Section 6.2.1. However, based on the SPOC and ISSA seismic profiles, the P-wave velocities are higher (Table 4.1) than would be expected for a felsic upper and/or middle crust (Table 4.2). A P-wave velocity of 6.6 km/s at 20 km depth, based on the ISSA profile (Figure 4.4), corresponds to a density of 2.9 Mg/m^3 and a P-wave velocity of 6.5 km/s at 20 km depth, based on the SPOC middle seismic profile (Figure 4.6), would give a density of 2.85 Mg/m^3.

A problem with a thin crust scenario is the depth of the crust/mantle boundary. The Moho in this scenario would be located where P-wave velocities from the local earthquake tomography model are in the range from 6.9 to 7.0 km/s below the volcanic arc, and from 7.0 to 7.1 km/s below the Longitudinal Valley. These velocities are too low to be associated with the crust/mantle interface.

The crust/mantle interface of a thick crust with a higher density in the lower crust, would reach depths, where P-wave velocities in the local earthquake tomography model are 8.0 to 8.1 km/s below the Longitudinal Valley. These values are too high because the crust/mantle interface in the local earthquake tomography is interpreted as the 7.75 km/s isoline.

For these reasons, the versions of the density model with modified lower crust cannot suitably define the crustal structure of the study region.

6.3 Varying parameters related to the oceanic plate

6.3.1 Slab density

The slab geometry, position, and density are important influences on the gravity field. The following tests show how the calculated gravity changes in response to density variations within selected parts of the slab. Each larger or smaller segment of the slab influences the gravity field regionally, and the magnitude is in many cases far bigger than the errors associated with the observed gravity data.

A density increase of +0.05 Mg/m^3 from the previously modelled density value of 3.3 Mg/m^3 in the oceanic crust of the subducting plate (Figure 6.15), affects the calculated gravity curve along its entire length. This density variation is rather small, but the regional extent of its effect demonstrates the importance of the density values assigned to the slab, despite the thinness of the oceanic crust.

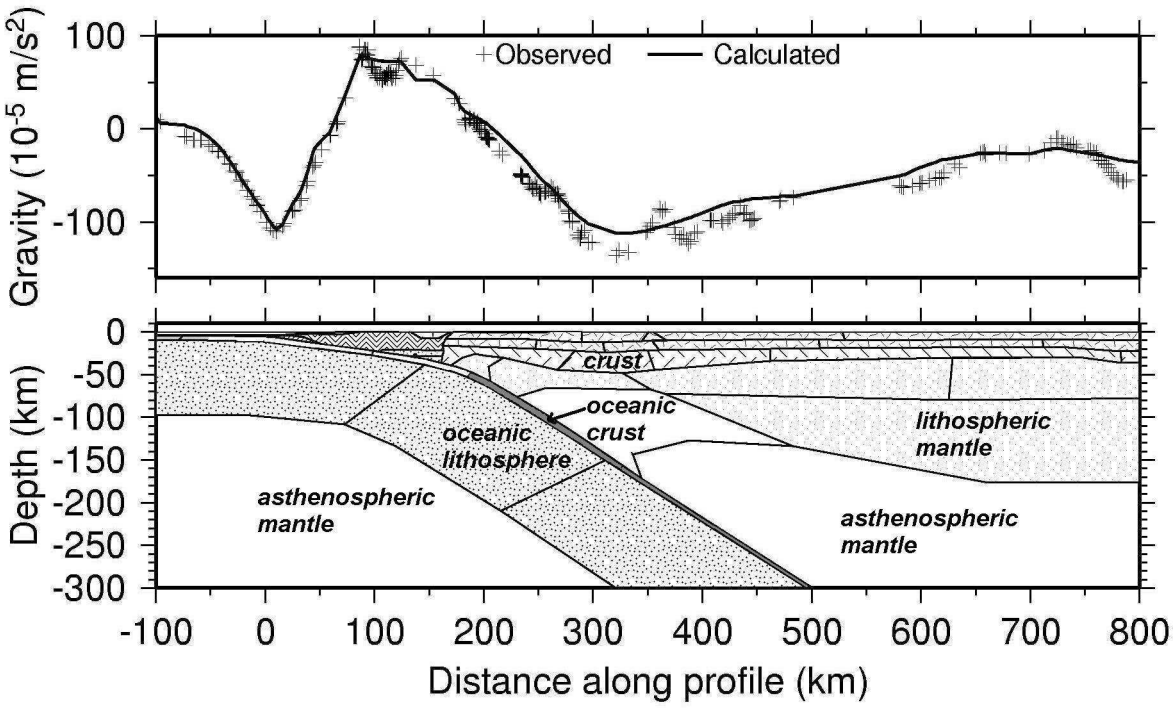

Figure 6.15
Effect on calculated gravity increasing the density of the subducting oceanic crust (gray) by 0.05 Mg/m^3.

The calculated gravity values are extremely sensitive to the slab densities and because the slab is a ubiquitous feature, it has to be thoroughly analyzed so as to derive the correct density values. Thus, the discussion of the composition of the slab crust and the lithospheric mantle, with the mineralogical transitions that occur at specific P/T conditions, is also significant. As shown in the following examples, variations in the thicker parts of the slab mantle and/or variations in density greater than 0.05 Mg/m^3, enormously influence the entire gravity field.

The deeper slab (lithospheric mantle) also significantly influences the modelled gravity curve. If the density of the slab below 150 km is increased by +0.05 Mg/m^3 the influence on the gravity curve extends from the trench to the backarc area (Figure 6.16). To compensate for this small density change, the entire crustal structure must be modified. The misfit of ~50×10^{-5} m/s^2 above the volcanic arc, requires a major change to the crustal structure in terms of both density and thickness. Likewise, a similar density change to the upper part of the slab (50–200 km depth) particularly influences the forearc gravity high (Figure 6.17).

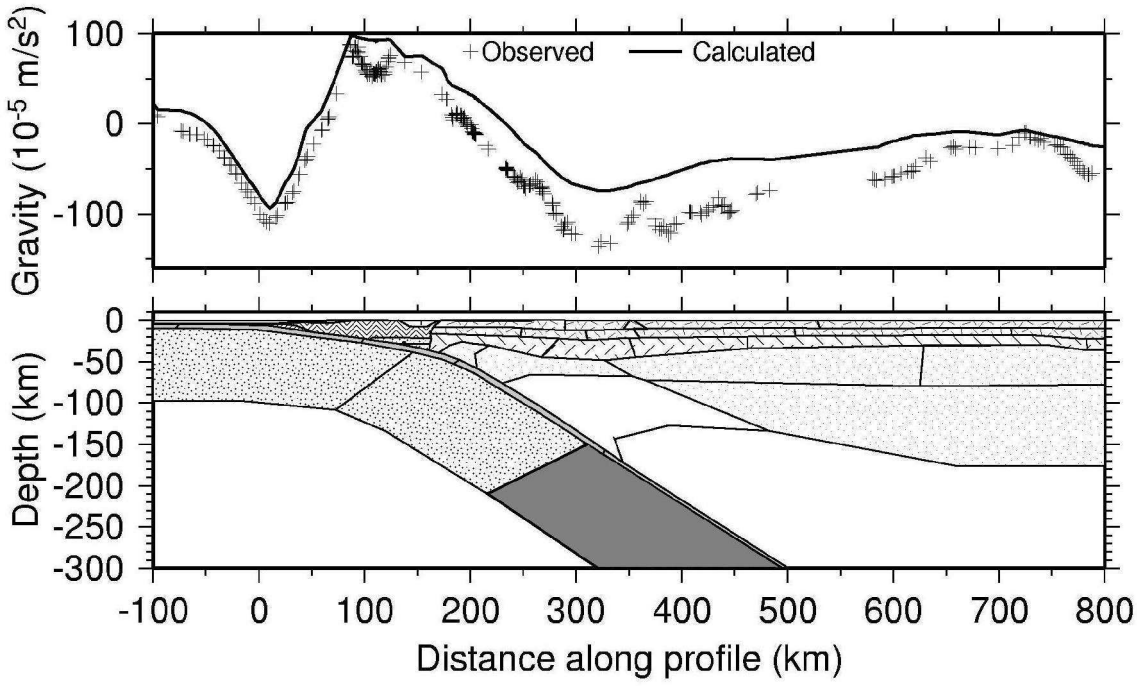

Figure 6.16
Effect on calculated gravity of increasing the density of the deeper part of the slab (gray shading) by 0.05 Mg/m^3. See Figure 6.5.C for a legend.

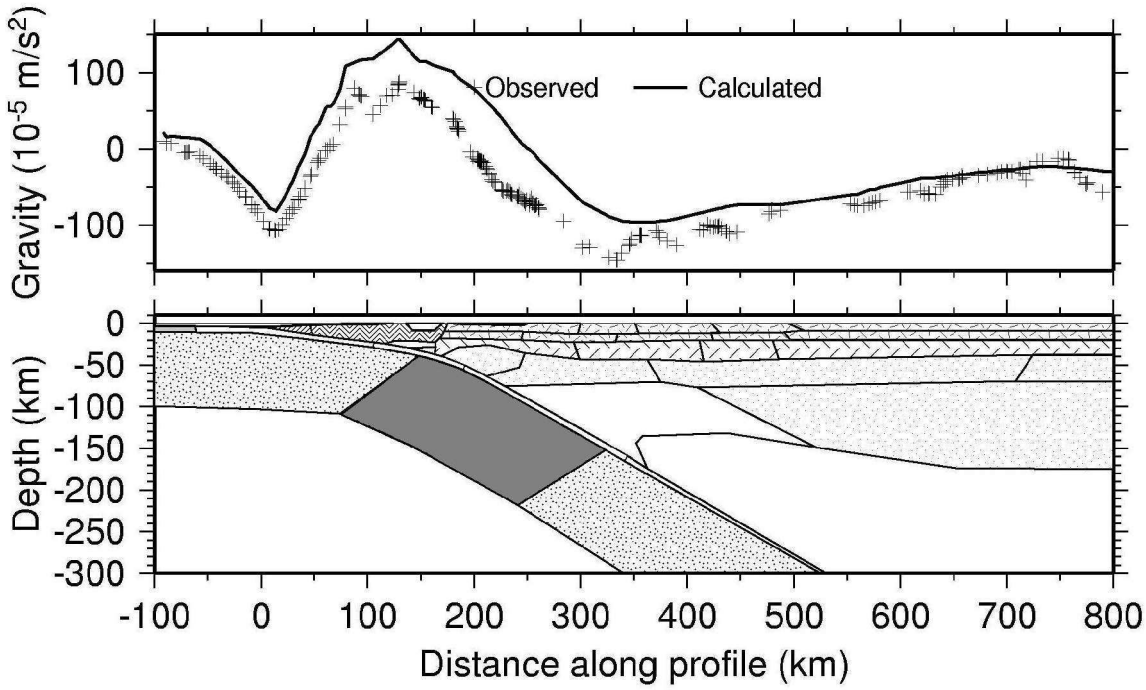

Figure 6.17
Effect on calculated gravity of a 0.05 Mg/m^3 increase in density for the upper part of the subducting slab. See Figure 6.5. C for a legend.

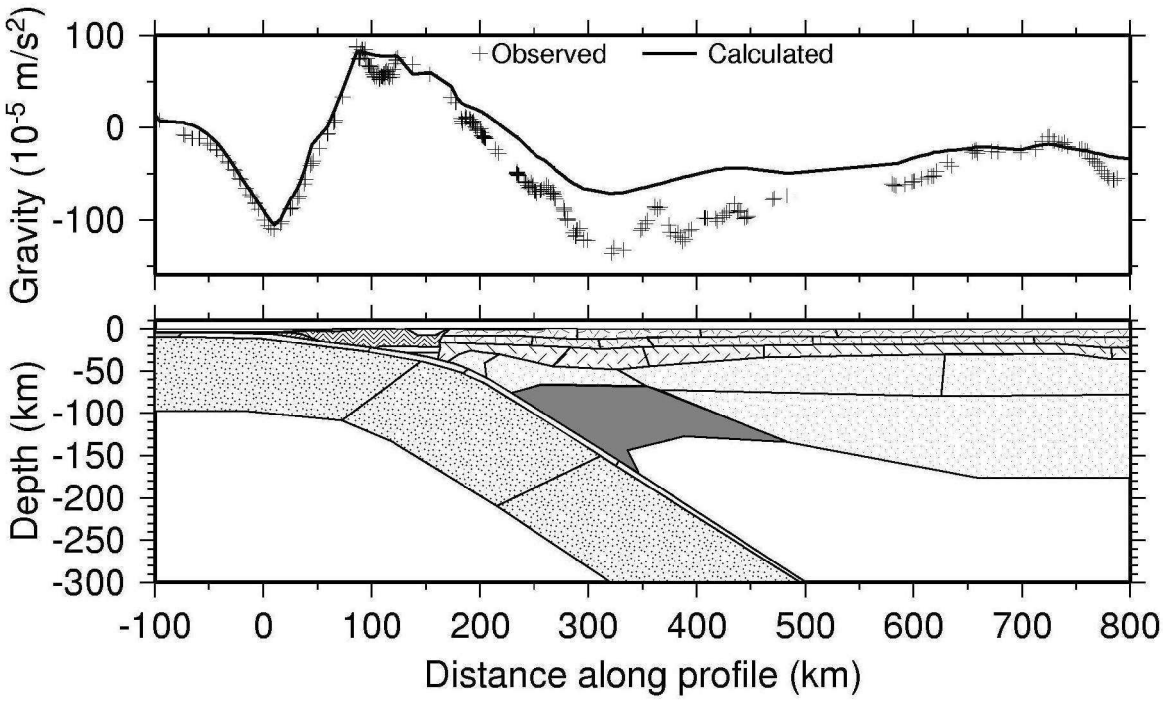

Figure 6.18
The effect of the asthenospheric mantle wedge. The density increase of 0.05 Mg/m^3 which, similarly to the slab, has a very strong influence on the calculated gravity field.

These modifications demonstrate how important it is to know the slab structure, but the underlying asthenospheric mantle is also important (Figure 6.18). Because the gravity field is greatly affected by the choice of slab density, the task of assigning correct density values within the oceanic plate is important also for modelling correct crustal parameters (geometry and density). A density variation of +0.05 Mg/m^3 in the deeper slab at 200 to 300 km depths (Figure 6.16) leads to an increase in the calculated gravity of 50×10^{-5} m/s^2. This would require a change in the crustal thickness of ~10–12 km and/or a density change of 0.05 Mg/m^3 for the lower crust. Therefore, constraints on the slab in the subduction zone cannot not be neglected in the density modelling.

6.3.2 The slab beneath the forearc (all three segments)

As shown in the previous section, the slab has a significant influence on the gravity and the structures of the overlying continental plate. The area south of 38.8° S (with no control on the slab position), is characterized by a deeper oceanic plate than in the Arauco-Lonquimay segment. This is valid if the assigned bulk density of the accretionary prism is correct. With a less dense forearc accretionary wedge, the corresponding mass deficit would have to be compensated for by a shallower slab. The following test (Figures 6.19 and 6.20) show two profiles from the Valdivia and Bahía Mansa-Osorno segments, where the calculated gravity field was well fit to the measured data in a modified model with a shallow slab, and a less dense accretionary wedge, and a deeper forearc basin than in the preferred (and final) model.

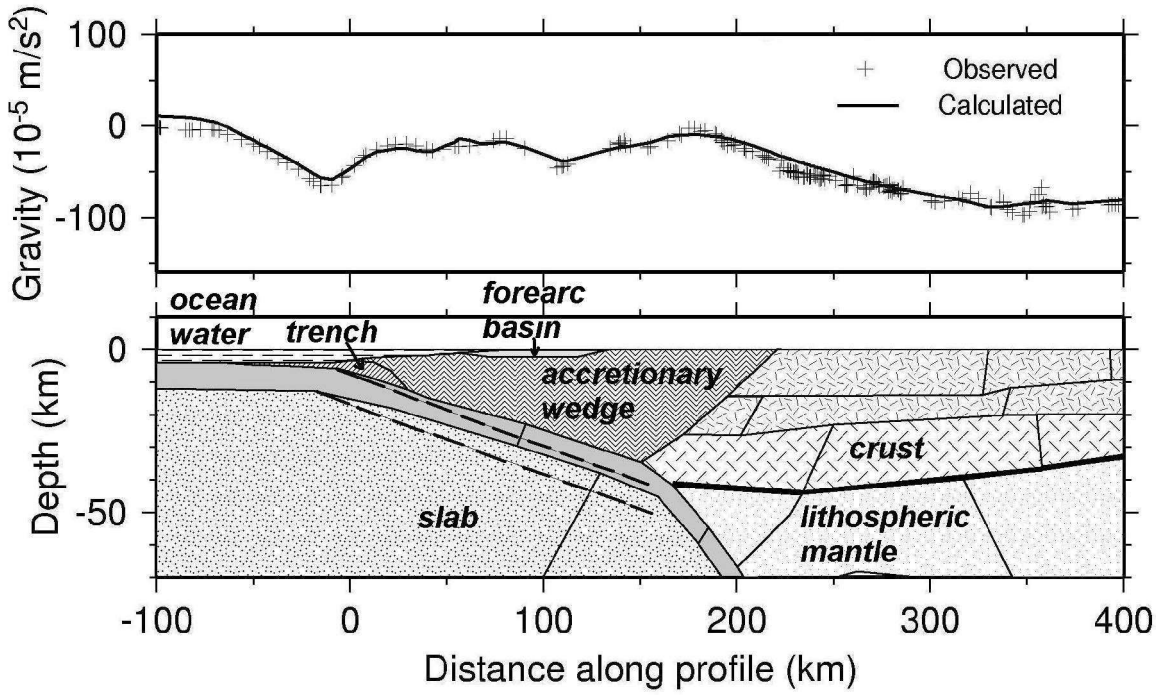

Figure 6.19
Model with a shallower slab in the Valdivia-Liquiñe segment. The calculated gravity reproduces the measured gravity if the density of the accretionary wedge is lowered to 2.8 Mg/m^3. The original depths of the oceanic plate are marked by dashed lines, and a thick black line denotes the crust/mantle interface.

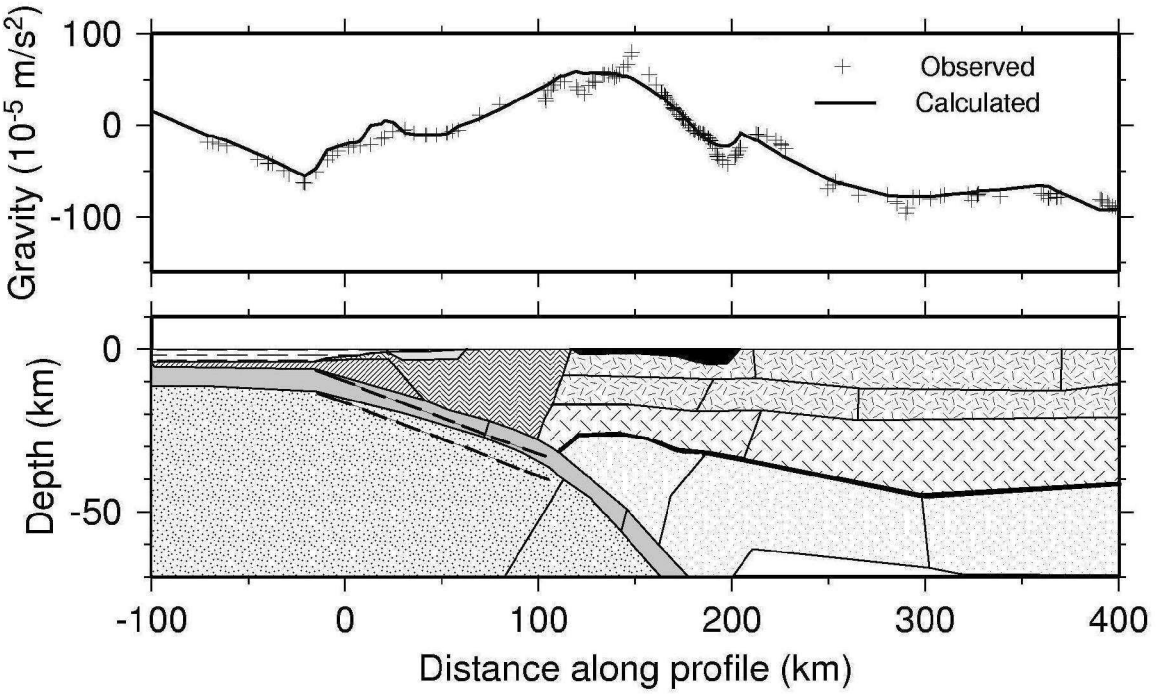

Figure 6.20
Model with a shallower slab beneath the Bahía Mansa-Osorno segment. The measured gravity field is reproduced if reduced density of 2.8 Mg/m^3 is used in the accretionary wedge. The original depths of the oceanic plate are marked by dashed lines, and a thick black line denotes the crust/mantle interface.

In these examples (Figure 6.19 and Figure 6.20), the density variation in the accretionary wedge is only -0.05 Mg/m^3. This requires the slab to shallow by 5 to 8 km. In the northern Arauco-Lonquimay segment, where the forearc and slab geometry are constrained by the seismicity and velocities of the four seismic profiles, the same density decrease would cause a significant reduction of the calculated gravity associated with the forearc region (Figure 6.21). Taking into account surficial geological observations and the assumption that the northern part of the accretionary prism should be less dense than the southern part, a density of ~2.75 Mg/m^3 was also tested (Figure 6.22).

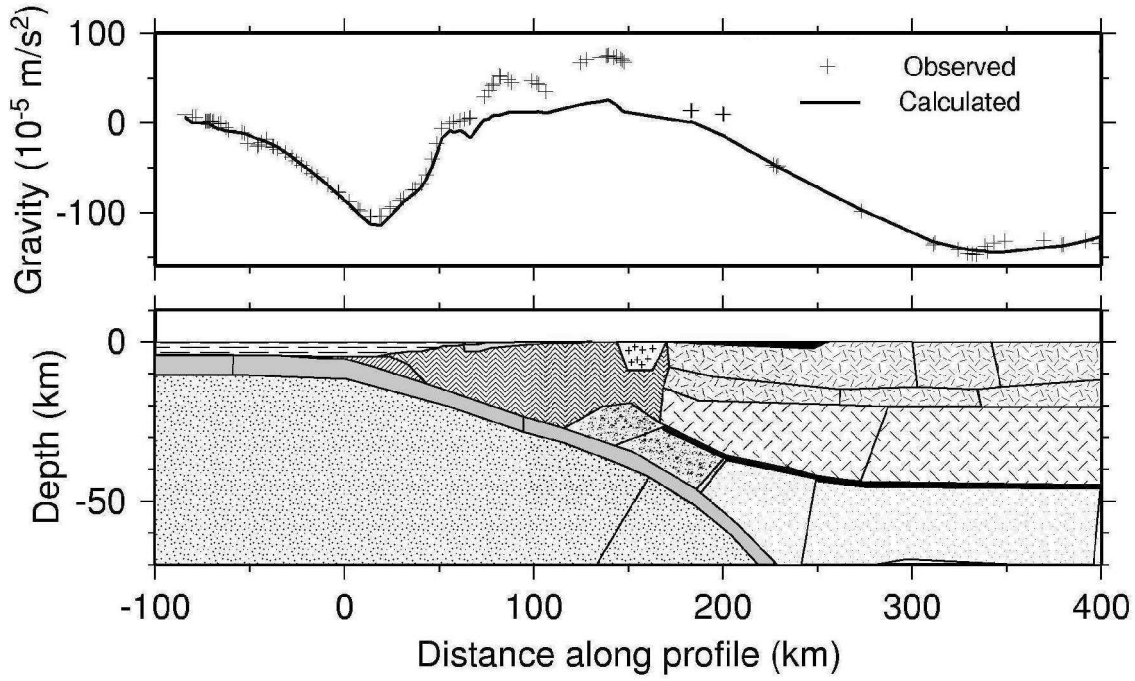

Figure 6.21

Effect of reducing density by 0.05 Mg/m^3 in the accretionary wedge of the Arauco-Lonquimay segment and its effect on the calculated gravity. The Moho is marked by a thick black line, and structures correspond to those in Figure 6.19 (see also legend in Figure 6.5.C).

In the case of the Arauco-Lonquimay segment, which is well constrained by velocity profiles and seismicity data, it is not possible to compensate the mass deficit caused by a less dense continental crust with a variation is slab depth. The only parameter that could affect the gravity is the density of the oceanic crust, which beneath the forearc in the density model is 3.1 Mg/m^3. The assumed crustal composition at these depths (30–60 km) corresponds to blueschist–amphibolite–greenschist facies, with densities ranging from 3.05 to 3.15 Mg/m^3 (Hacker et al.,2003 and 2004). These values, or even a higher value of 3.3 Mg/m^3 within the

oceanic crust are not sufficient to replace the missing mass caused by a less dense (2.75–2.8 Mg/m^3) accretionary wedge.

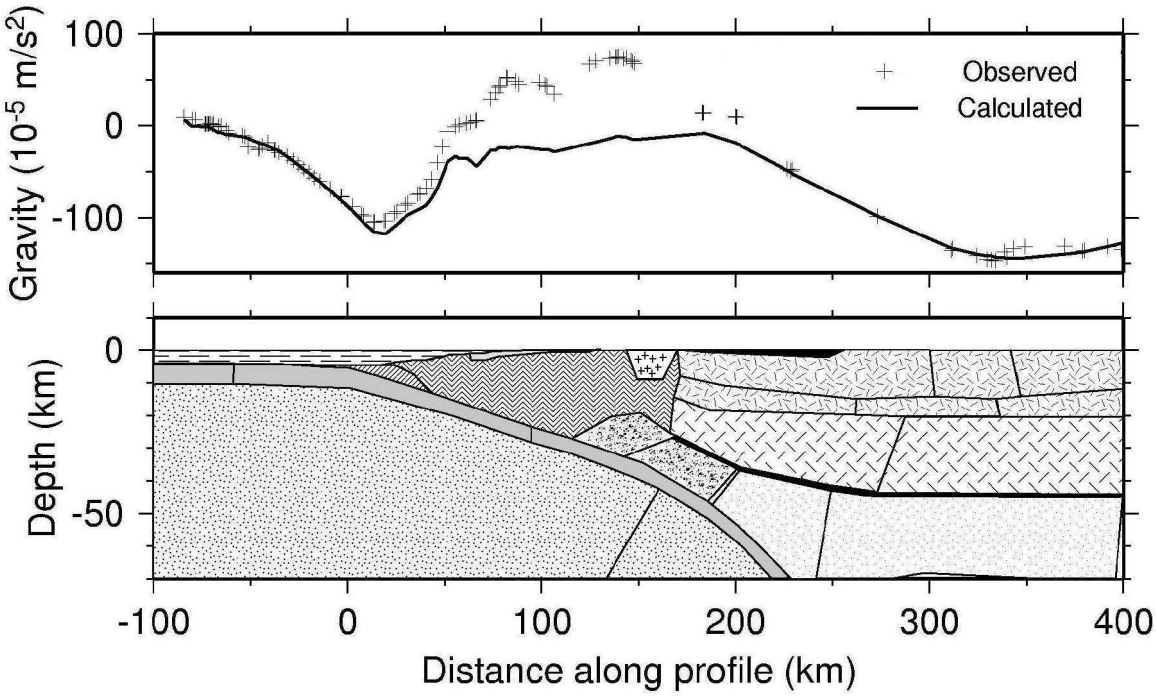

Figure 6.22
Effect of reducing density by 0.1 Mg/m^3 in the accretionary wedge of the Arauco-Lonquimay segment and its effect on the calculated gravity. The Moho is marked by a thick black line, and structures correspond to those in Figure 6.19 (see also legend in Figure 6.5.C).

6.3.3 The slab under the Arauco-Lonquimay segment

The influence of the oceanic plate geometry and depth on the gravity high within the Arauco-Lonquimay segment was tested (Figure 6.23). First, a 5 km deeper slab was modelled systematically on all profiles of 36–39°S. The resulting calculated Bouguer anomaly is displayed in plan in Figure 6.25, where it is shown that almost 70% of the positive Bouguer anomaly value has disappeared.

A.

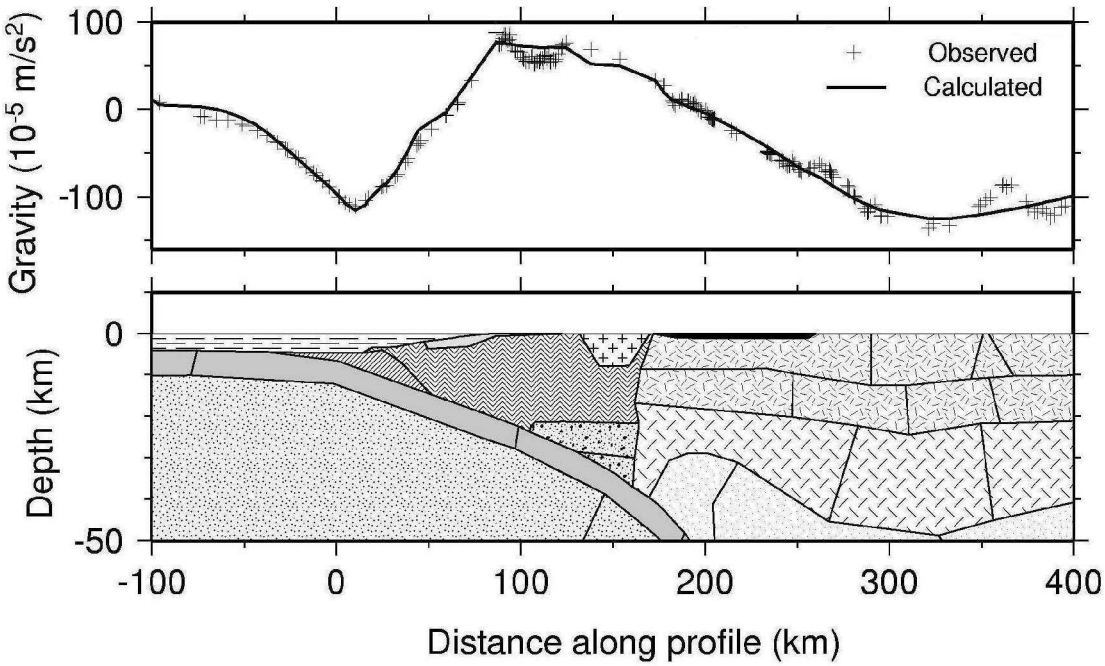

B.

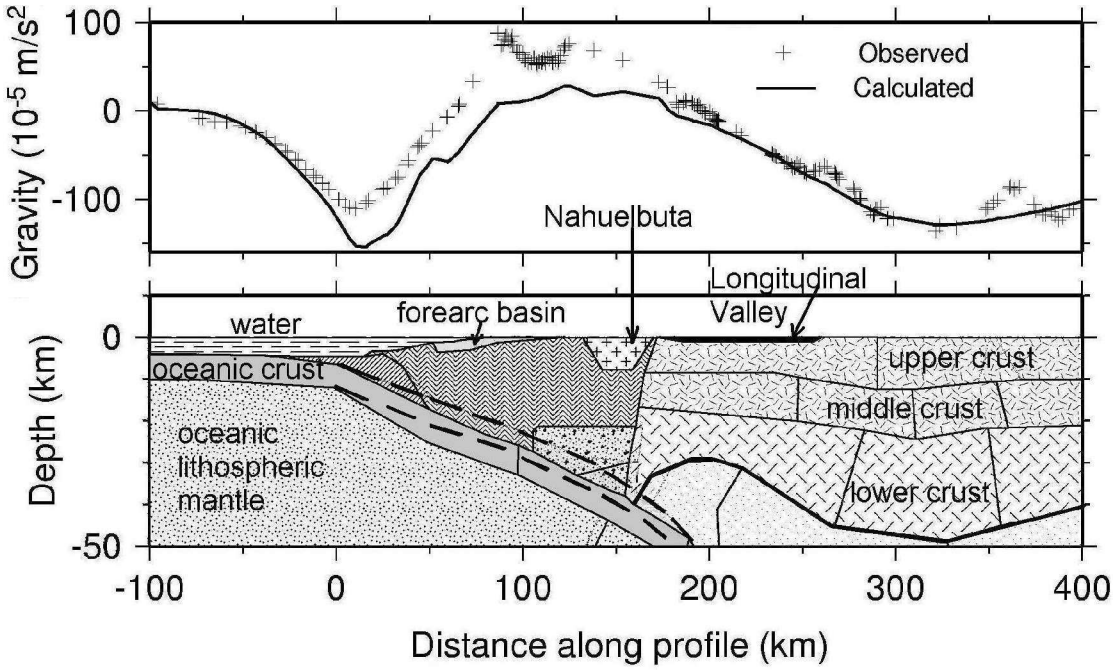

Figure 6.23
The change of the calculated anomaly related to the change of the oceanic plate depth.
A. The original structure along the profile at ~ 37.3°S
B. The plate was shifted 5 km deeper in the area of 0–150 km distance along the profile. The initial position of the slab is indicated by the dashed lines and the Moho boundary is indicated by a thick black line.

The apparently strong influence of a deeper slab on the gravity high may also partly cover the influence of other bodies. Therefore, the same test was also done with the crust/mantle boundary, whose depth was likewise decreased by 5 km. This change was applied while maintaining the original geometry of the slab in order to show only the effect of the depth of the crust/mantle boundary underneath the Longitudinal Valley in the gravity field (Figure 6.24).

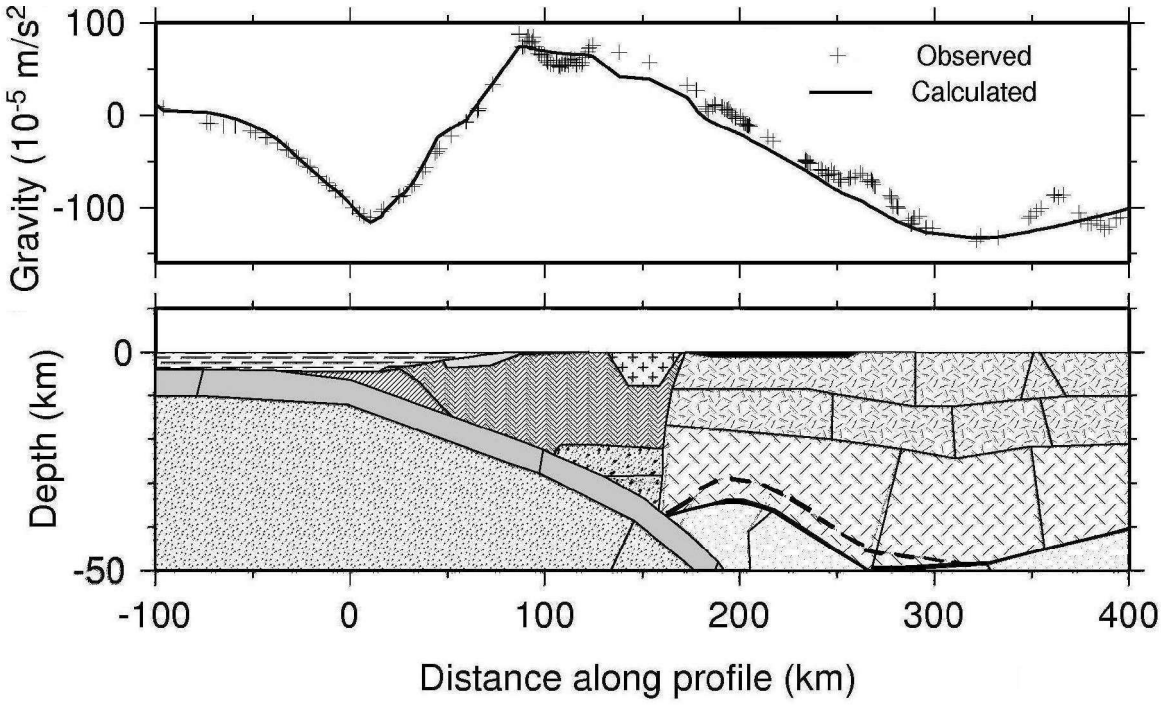

Figure 6.24
The change in calculated anomaly caused by a 5 km deeper crust/mantle interface. The original anomaly along the same profile is shown in Figure 6.23 A. The shallower mantle below the Longitudinal Valley was modelled 5 km deeper between 150 to 250 km along profile. The the position of the slab remained unchanged. The initial Moho boundary is indicated by a dashed line and the shifted position by a thick black line.

The maps of the measured Bouguer anomaly together with calculated gravity (Figure 6.25) also show the influence of the changes in slab and Moho position. The effect of deepening the Moho is not as strong as that of deepening the oceanic plate position, but it still has an important impact on the shape and magnitude of the anomaly in a more local sense.

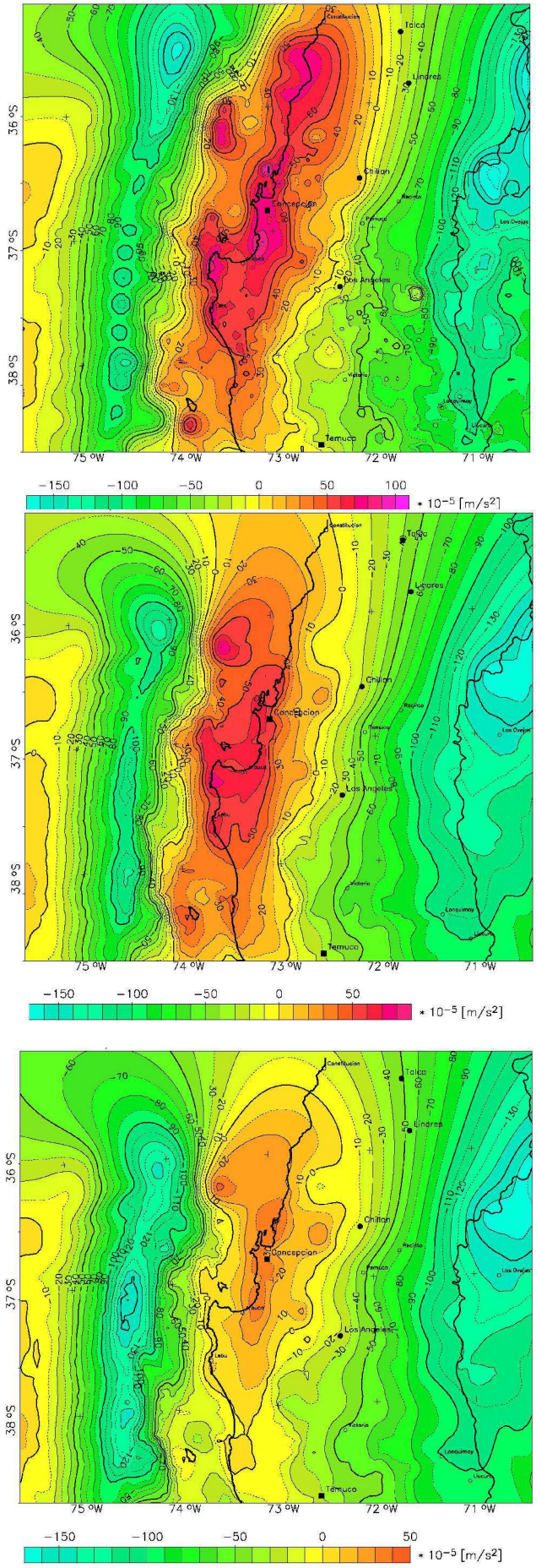

Figure 6.25
The original gravity field (A) compared to the calculated Bouguer anomaly with the Moho below the Longitudinal Valley 5 km deeper than modelled previously (B), and also with the slab 5 km deeper below the forearc (C). The slab has a much stronger effect on the gravity, but the position of the crust/mantle interface, below the Longitudinal Valley also contributes to the gravity high observed in the forearc of the Arauco-Lonquimay segment.

A. measured Bouguer anomaly.

B.
the influence of the crust/mantle interface.

C.
the influence of the slab depth.

One last body influencing the positive Bouguer values within the Arauco-Lonquimay segment, but only at short wavelengths is a body of uncertain affinity, previously called unidentified body (pink, Figure 6.26), discussed in Section 6.1.3. It exists at the bottom of the accretionary wedge and has a density of 3.15 to 3.2 Mg/m^3, adding about 30 to 40×10^{-5} m/s^2 to the calculated anomaly. The following image shows which parts of the model contribute to which parts of the observed gravity.

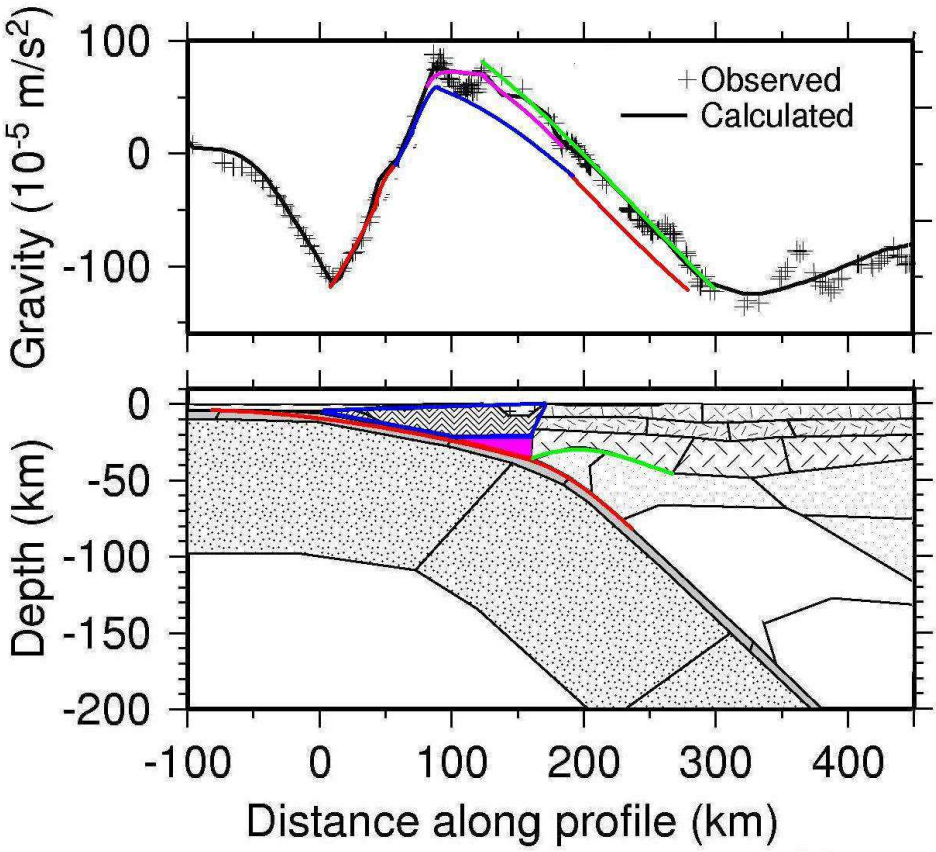

Figure 6.26
Influence of different structures on different parts and wavelengths of the gravity curve, as it is interpreted in the final density model. The effect of all four segments supplement each other in both, wavelength and amplitude. The position of the slab controls the wavelength (red line), and the crustal structures of the continental plate the magnitude of the gravity anomaly (blue and pink lines). The crust/mantle interface influences both (green line).

6.3.4 The slab and the crustal thinning south of 40°S

Compared to the Arauco-Lonquimay segment, the southern Bahía Mansa - Osorno segment (40–41°S) is characterized by a deeper oceanic plate (~35 km) below the forearc, and shallower mantle below the Longitudinal Valley. The geometry of the slab was therefore changed here in order to test different possibilities for the source of the gravity anomaly. The slab was modelled ~5 km shallower, reaching similar depths to the Arauco-Lonquimay segment, and the geometry of the crust/mantle interface was simultaneously deepened, thus testing the hypothesis that the positive anomaly is caused by the oceanic plate rather than the shallow mantle. The shallower oceanic plate only fits the positive gravity anomaly (in the vicinity of the Longitudinal Valley), but because the plate influences the long wavelength parts of the gravity field, this change brings mass also into the region, which has in the measured gravity field negative values. The resulting peak in the modelled Bouguer anomaly is then shifted westwards and the misfit between the calculated and measured anomaly is 30 to 50×10^{-5} m/s^2 (Figure 6.27 B.). By lowering the density of the accretionary prism (by 0.05 Mg/m^3), the calculated curve could be adjusted to the measured one.

However, doing so gives a slightly worse fit over the gravity maximum. When the crust/mantle interface was shifted back to its initial position (shallow depths below the Longitudinal Valley), combined with a less dense accretionary wedge and a shallow oceanic plate, the gravity field was well reproduced. Therefore, the anomaly south of 40°S is interpreted to dominantly reflect the shallow mantle, not the position of the oceanic crust.

However, because of the lack of other geophysical data in this region, another possibility was tested. The observed gravity field can be reproduced using a denser crust than in the two northern segments. This version of the model has a normal crustal thickness (40 km) below the Longitudinal Valley with a denser middle and lower crust, 2.9 and 3.16 Mg/m^3 respectively (Figure 6.28), whereas in the original model, the positive Bouguer anomaly above the Longitudinal Valley south of 40°S was modelled with a thin crust (~25 km) of normal density (2.85 and 3.1 Mg/m^3 for the middle and lower crust respectively). The gravity field of the modified model was well reproduced and the modelled fields of the two versions (original and a modified one) were then analyzed using the curvature technique and compared to the measured data. The results are shown in the following section.

A.

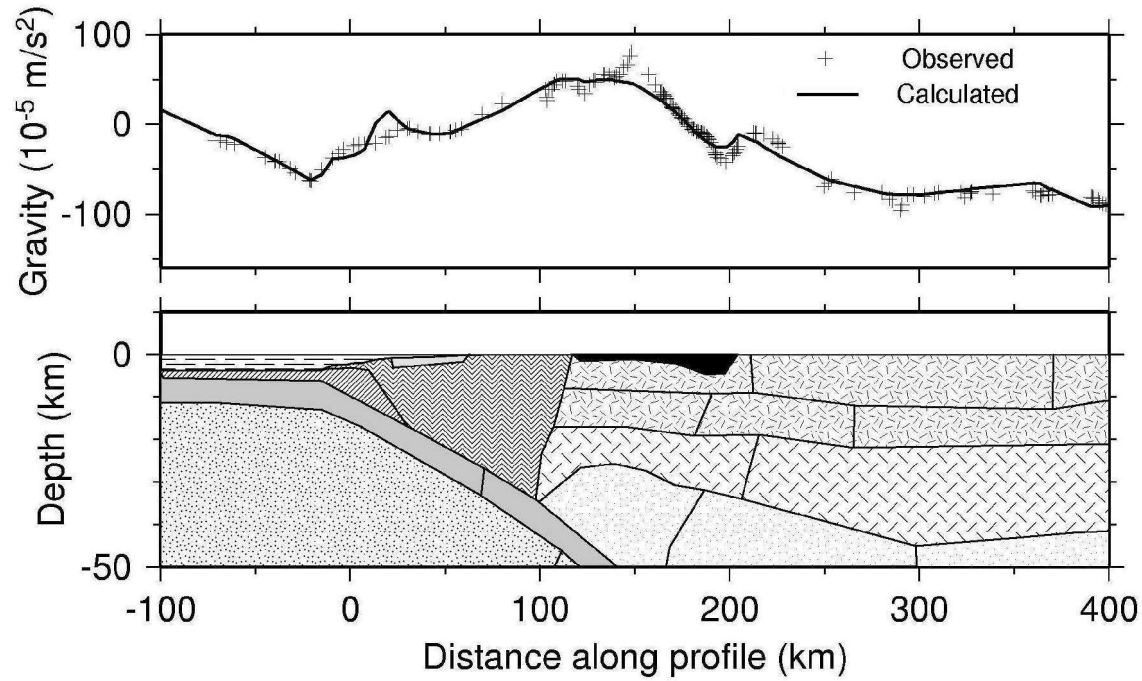

B.

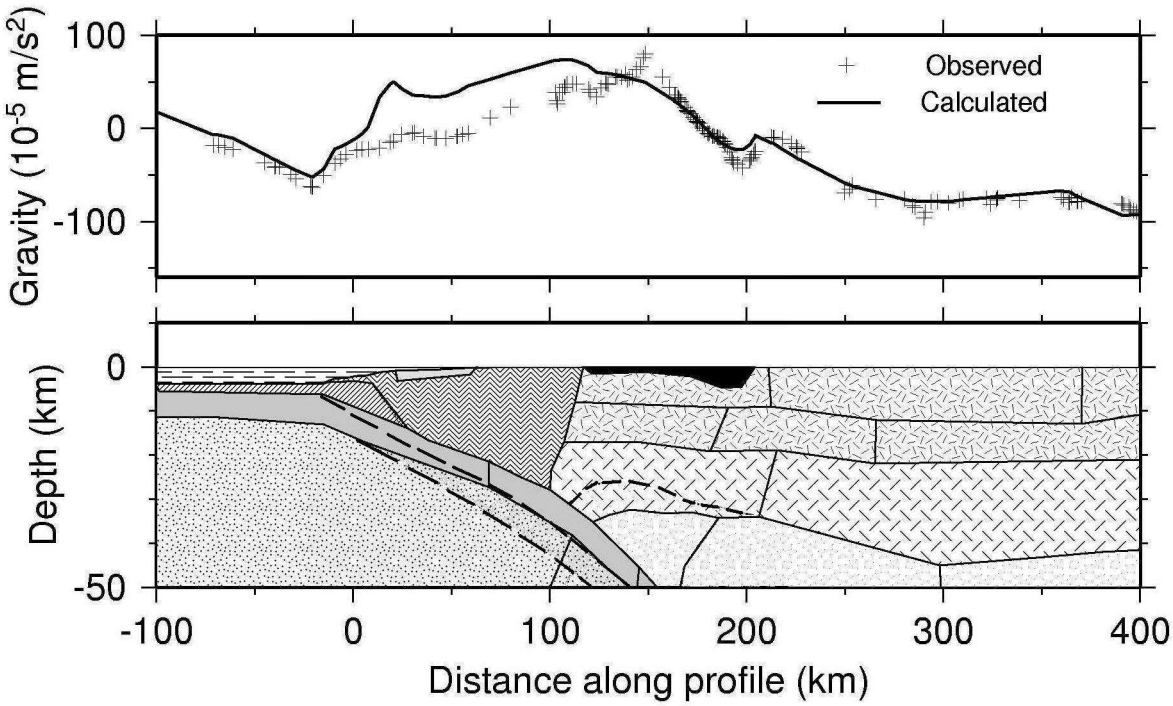

Figure 6.27
A. The original structure along the profile at ~ 41.3°S
B. The shallow plate and thicker crust below the Longitudinal Valley along the same profile. The initial position of the slab and Moho is indicated by the dashed lines.

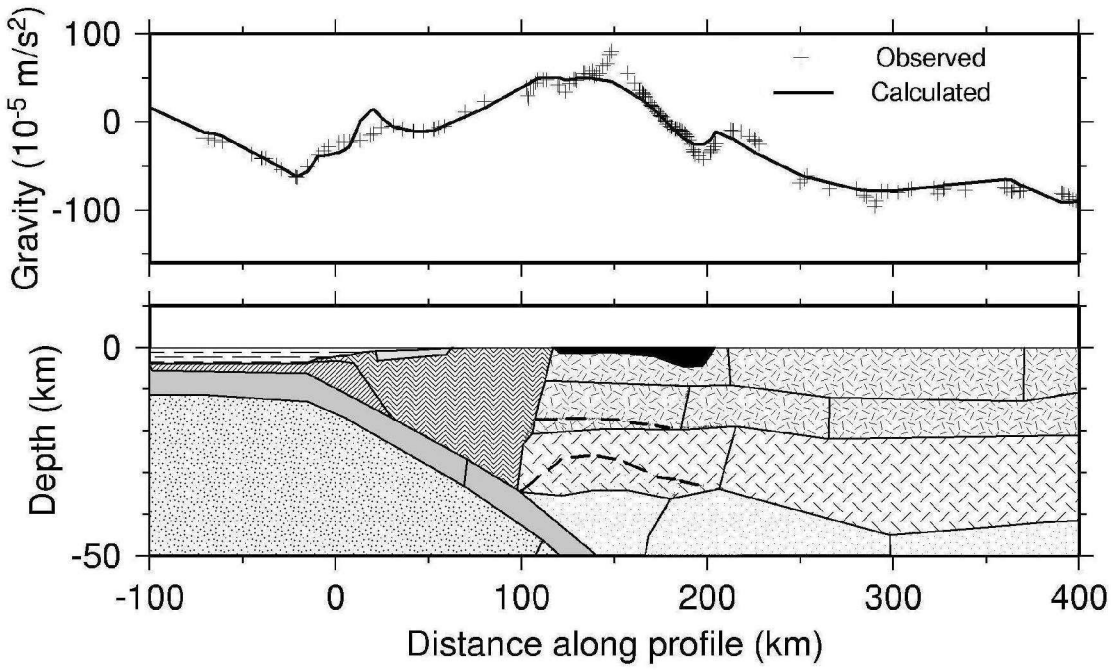

Figure 6.28
The observed anomaly here is reproduced by a dense crust and a normal crustal thickness of 40 km below the Longitudinal Valley. From a modelling point of view, this version is also possible because the modelled field is characterized by the same standard deviation from the measured one as the preferred version of the model (Figure 6.27A). The initial position of the Moho and middle crust is indicated by dashed lines.

6.4 Curvature technique

Curvature is a 2D attribute of a curve that describes how much the curve deviates from a straight line and how bent the curve is at a particular point. Considering a point P on a curve (Figure 6.29), the curvature K is defined as the rate of change of angle dω with respect to the arc length *dS*:

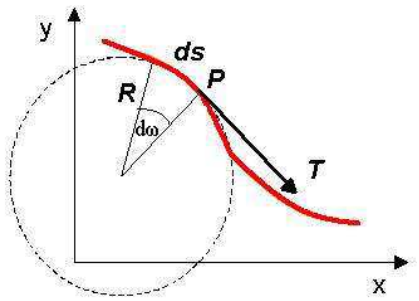

$$K = \frac{d\omega}{dS} = \frac{2\pi}{2\pi R} = \frac{1}{R} \quad (6.1)$$

Figure 6.29
All the elements necessary to define curvature at a point P.

The circle, whose radius R is the reciprocal of the curvature, has a common tangent T at the point P. The circle, which makes the greatest possible contact with the curve, is called the osculating circle. Any circle has a constant curvature K along its circumference.

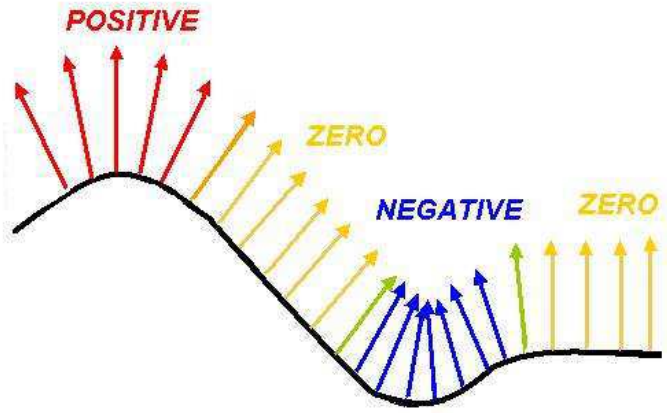

Figure 6.30

The vectors, which are normal to the surface, are shown at regular interval along the curve. Where they all are parallel to each other, the horizon has zero curvature (yellow)and is flat or planar. Where the horizon forms an anticline or a ridge feature, the vectors diverge (red) and the curvature is defined as positive. Where the vectors converge, the curvature is negative (blue) and the horizon forms a syncline.

The curvature is a surface-related attribute (Figure 6.30), which can bring insight into a particular aspect or property of the surface , which would be otherwise difficult or not possible to observe. It is closely related to the second derivative of the surface, but its quality is dependent on the level of noise. Curvature has previously been used for seismic data (Roberts, 2001), but has also been applied to and tested on potential field data (magnetic and gravity) (Schmidt, in-house software, pers. comm. 2002; and Kollersberger, pers. comm. 2004).

In this study, the curvature technique was used to compare the gravity field produced by a 3D model to the original measured field, in order to determine how well the calculated field fit the curvature attributes of the measured field. Also, the curvature analysis allowed a test of two different versions of the 3D density model to find which modelled gravity field is better adjusted to the observed field. The two alternative models (Figure 6.27A and Figure 6.28) fit the observed field equally well, but are based on different geometry and density characteristics. Various curvature attributes, presented below, were compared to detect faults and other features within the potential field that are not visible in the Bouguer gravity anomaly field itself. The following curvature attributes can be defined:

Minimum curvature (Figure 6.31) (and also the maximum curvature) contains information about fault-zone geometries and also their orientation. The locations where non-isometric distortions of the surface occur and where the surface is fractured and faulted, are characterize by large values of the minimum curvature.

Most positive curvature (Figure 6.32) is an attribute that shows the most positive curvature value of all possible normal curvatures. This attribute does not show shape information, but indicates the magnitude and presence of almost all possible lineaments.

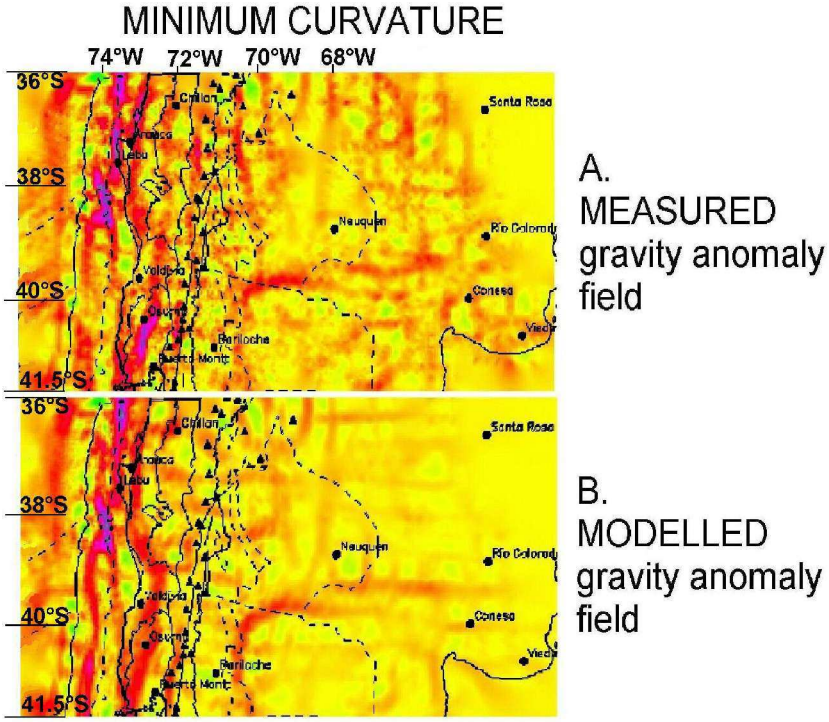

Figure 6.31
Minimum curvature overlain by, from left to right: Mocha and Valdivia Fracture Zones; trench; continental slope/shell boundary; coastline; Longitudinal Valley; volcanoes along the Liquiñe-Ofqui Fault Zone and the boundaries of the two morphological units - Neuquén basin and North Patagonian massif. The curvature of the field produced by a density model (B) of the preferred model (6.27 A) is compared to the curvature of the measured field (A).

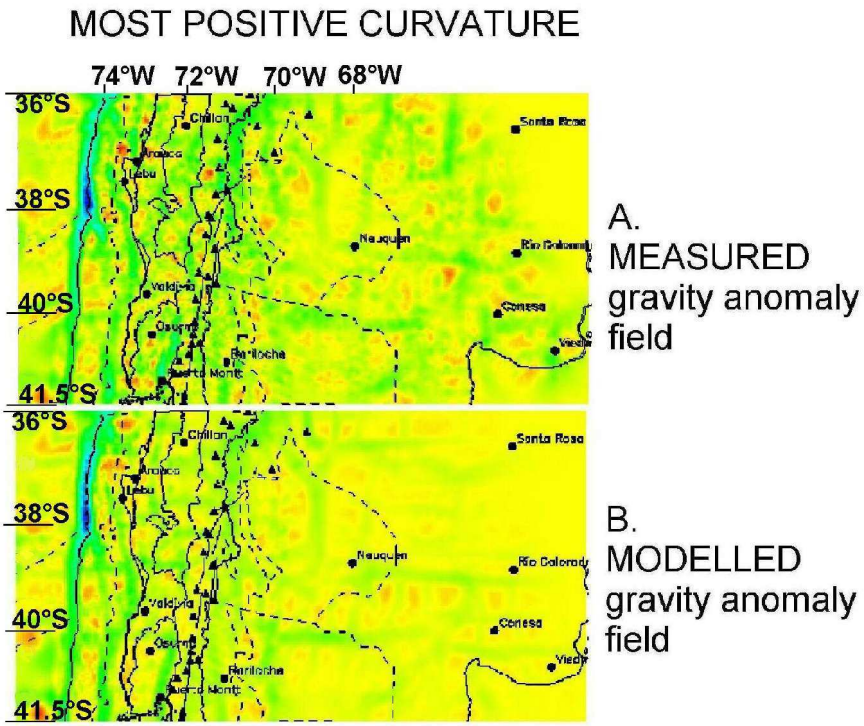

Figure 6.32
The curvature attribute most positive curvature. Most of the features observed in the curvature of the measured field (A) are reproduced well in the calculated field (B) of the preferred model (Figure 6.27 A). Some features are missing and/or show different values because detailed structures and possible errors in the data are not always modelled.

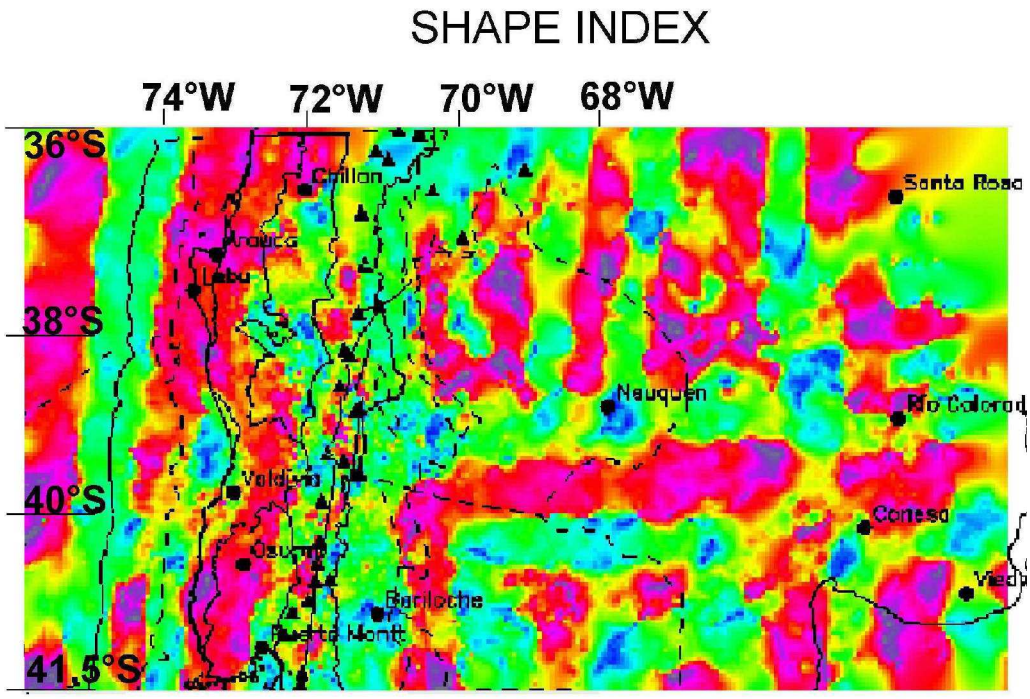

Figure 6.33
Shape index represents the form (shape) of local structures. These, in many cases, have a N-S trend, with the one E-W exception in the Neuquén basin. The red colour indicates a convex structure (e.g. crust/mantle upwelling) and green/blue colours indicate a concave shape (e.g trench).

Shape index (Figure 6.33) is used for a quantitative description of the shape, describing the morphology of a local surface, independent of the scale. This attribute is not influenced by the absolute magnitude of curvature and therefore minor faults, surface patterns and lineaments can be enhanced.

Dip curvature (Figure 6.34) is a measure of the rate of a change of the dip in a maximum dip direction. The magnitude and the direction of faults is preserved. This attribute can be used to improve detection of compacted features (channelized bodies), and tends to exaggerate any local relief contained within the surface.

Azimuth and Dip angle (Figure 6.35) are useful for detecting edges associated with asymmetric faults and/or symmetric ridges/valleys; therefore these attributes are useful for the interpretation of the surface features.

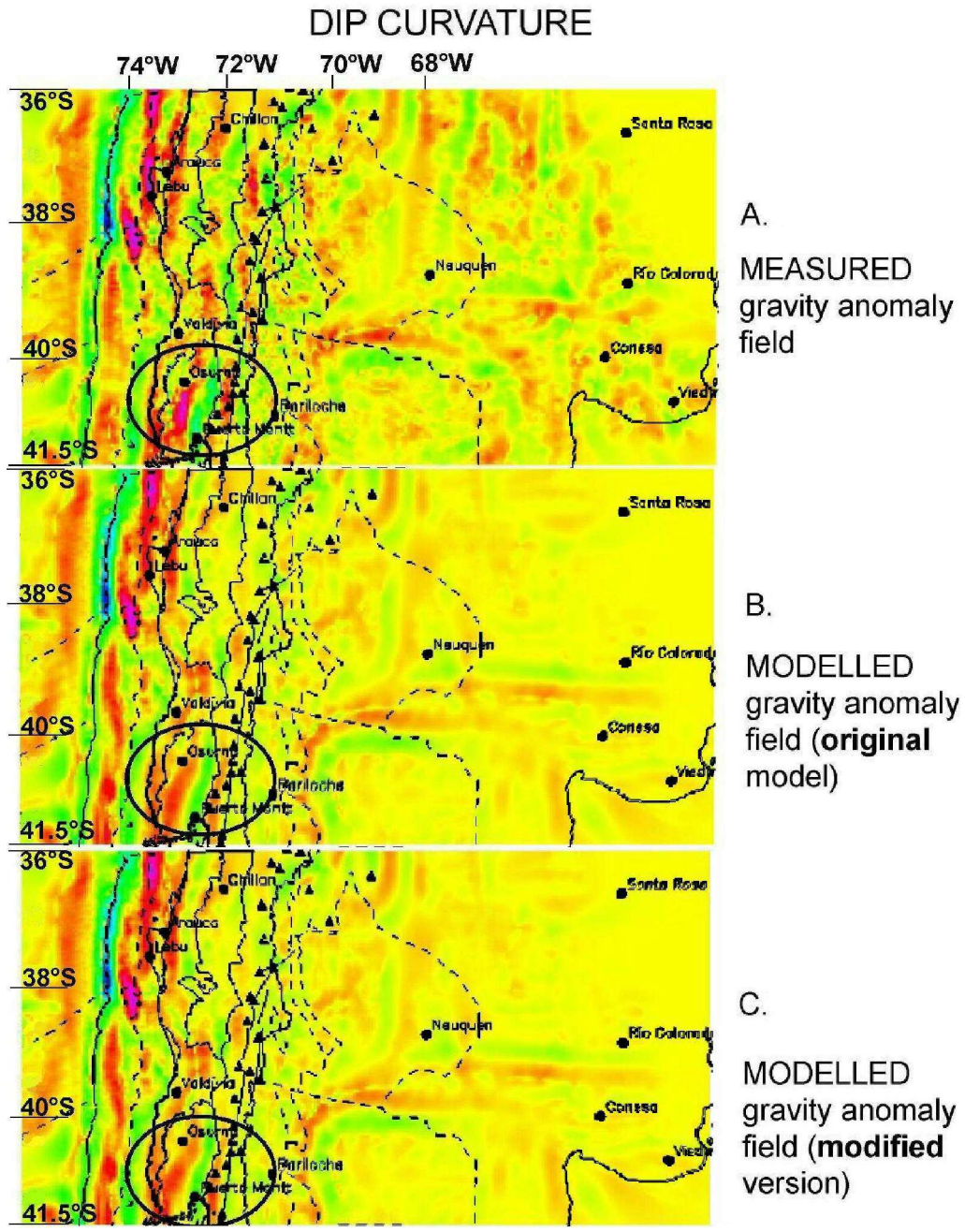

Figure 6.34

The measured field (A) with dip curvature compared to the two modelled versions, where (B) is based on the preferred model (Figure 6.27A) and (C) on the modified version (Figure 6.28), in which the gravity high in the Bahía Mansa-Osorno segment was modelled by a thick and dense crust. The differences in the areas of interest (black ellipses) are found in front and along the volcanic arc, where in the second image the green boundary between the two red spots in the Osorno-Puerto Montt area is slightly better reproduced than in the third image. There, the green boundary at Osorno is too thin and the positive values below the last volcanoes are not high enough.

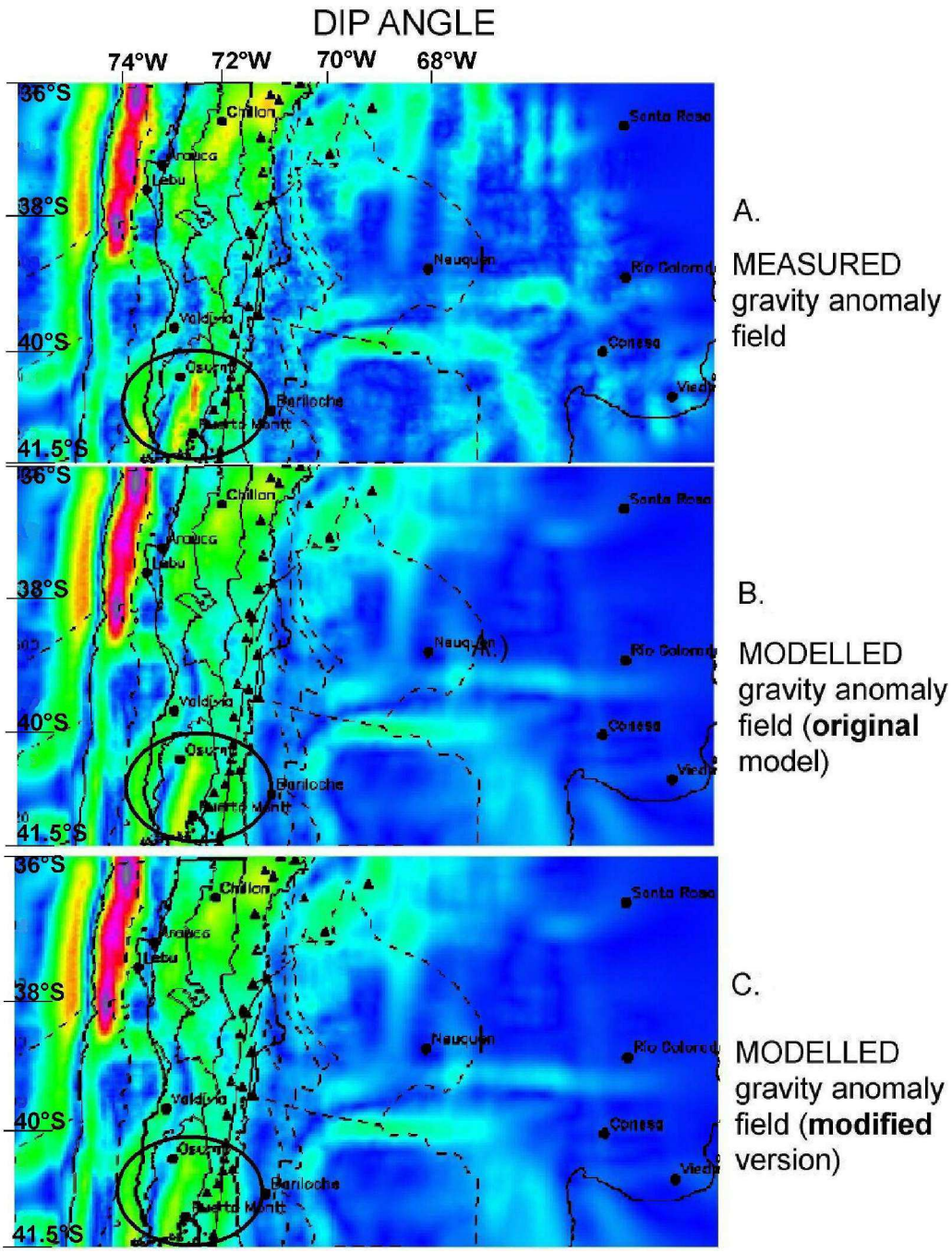

Figure 6.35

The measured field (A) with a curvature attribute dip angle compared to the two modelled versions (Figures 6.17A for the original model and 6.18 for the modified version). The differences in the areas of interest (black ellipses) are found along the volcanic arc. In the second image (B) the blue boundary between the two green areas at Osorno-Puerto Montt is not fully, but still better, reproduced than in the third image (C), where almost all is green, indicating less negative values than within the measured field.

Results of the curvature

There are some general features observable in the results from all 6 curvature attributes. The best results are for minimum curvature (Figure 6.31) and the dip angle (Figure 6.35), whose minimum values highlight the trench and the continental slope/shelf transition. The concave shape of the trench is also detected by the shape index (Figure 6.33). All the curvature attributes show N-S trending features along the coastline, volcanic arc (positive values of most positive curvature, shape index and dip curvature: Figures 6.32–34) and in the eastern part of the study area. Also prominent, especially in the minimum curvature, dip curvature, shaded relief (Figure 6.36), azimuth and partly also in the shape index attributes, is an E–W feature of the southern margin of the Neuquén basin. This feature is also seen within the residual isostatic field (Figure 5.12)

This E–W feature is also seen in the Bouguer anomaly field (Figure 6.36) and also in the density model (Figure 5.19), which agrees with the convexity of the feature seen in the attribute shape index (Figure 6.33).

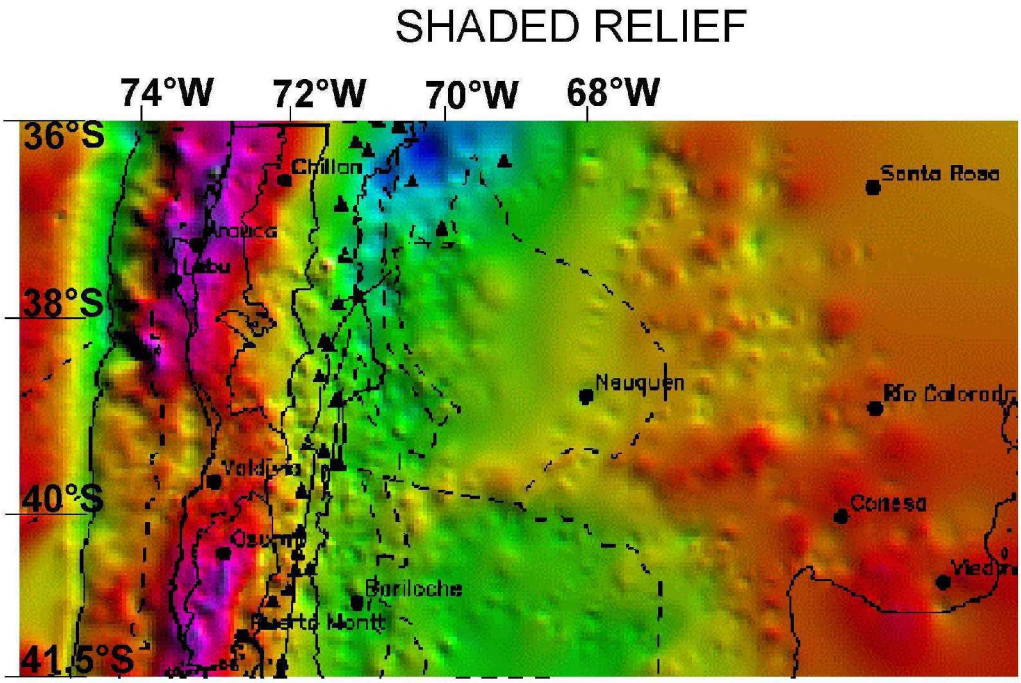

Figure 6.36
The measured gravity field as a shaded relief.

In general, both fields reproduced from the two models (original and modified) show a good fit with the measured gravity (apart from the southern

segment of the second version) in all applied curvature attributes, despite local misfits. These may be due to error contamination of the measured data or to local anomalies that are not reproduced by the models.

The major differences in the geometry of the calculated gravity field of the two alternative models in Figures 6.27 A and 6.28, are well seen using minimum curvature, dip curvature (Figure 6.37), also partly using dip angle and most positive curvature. The results show that the detailed features, not easily seen in the cross sections of the gravity anomaly field, has been reproduced better in the model with thinned crust (original model) than in the one with normal crust (modified model).

However, the curvature attributes do not validate the modelled features. They can only determine small differences in curvature characteristics between the models, even though the overall accuracy of both versions is essentially the same.

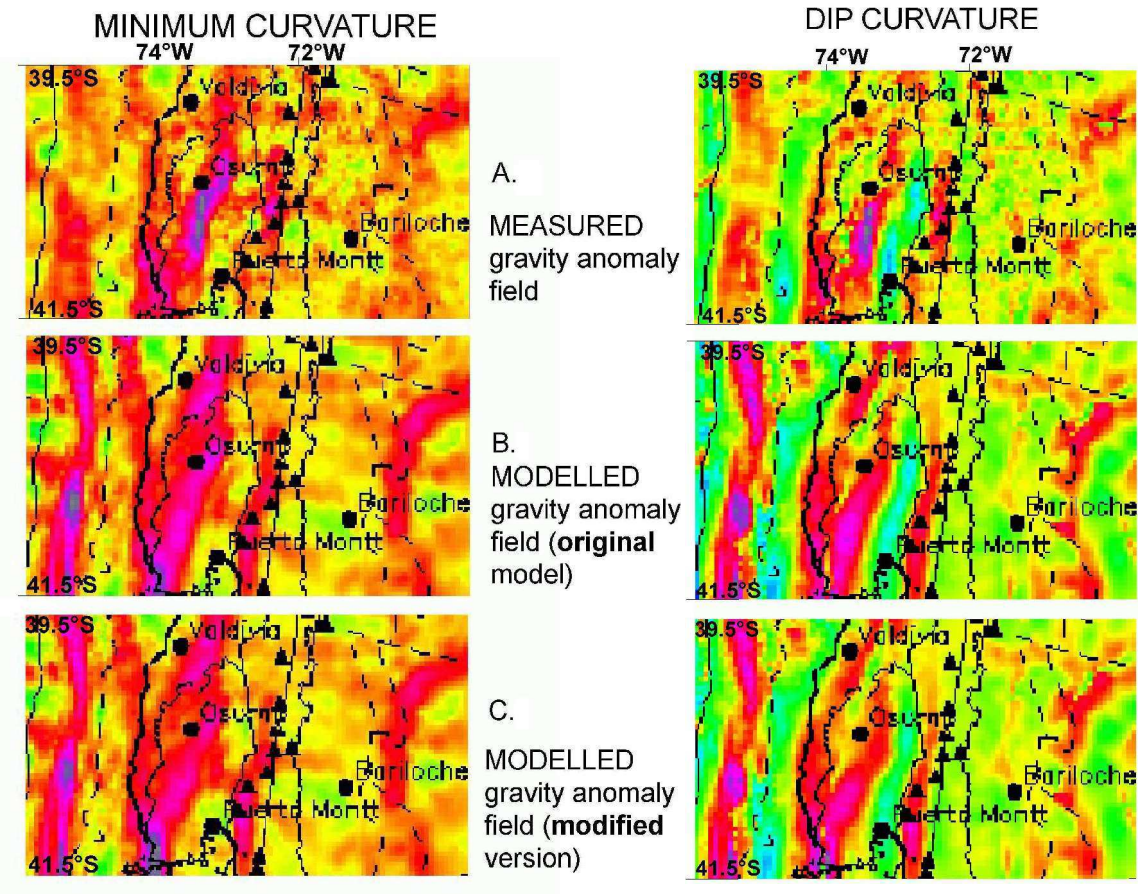

Figure 6.37

Detailed sections images of minimum & dip curvature for the modelled gravity field from the two alternative models (B & C) of Figures 6.27 A and 6.28 compared to the curvature of the measured data (A). The differences between the two models occur at: the Osorno-Puerto Montt area where, in the dip curvature, the light-blue - green boundary, indicating a medium dip, is better reproduced in the preferred version of the model (with a thinner crust); and around Puerto Montt where, in the minimum curvature, this spot is also better reproduced in the first version of the model. The differences are small, but are observable in three attributes (minimum curvature, dip curvature and dip angle, also in Figures 6.34 and 6.35).

6.5 Conclusions

Based on the gravity dataset, characterized by an accuracy of 5–10×10^{-5} m/s^2 in the Bouguer anomaly, and the 3D density model developed in the framework of this thesis, the following results may be concluded for the three segments. They are recognized within the gravity field and are also based on geological observations.

The gravity high in the Arauco-Lonquimay segment at 37–39°S is caused by a shallow oceanic plate under the forearc together with crustal thinning associated with the Longitudinal Valley. A structure of uncertain affinity at the base of the forearc accretionary wedge, also appears to influence the gravity field. This is the only segment where other geophysical data are available.

A positive Bouguer gravity anomaly is absent in the Valdivia-Liquiñe segment, in contrast to almost the entire South American margin. It is due to a relatively deep oceanic plate and a lack of crustal thinning below the forearc where the Longitudinal Valley is absent. As well, the unidentified body in the forearc is not observed south of 39°S. Therefore, the mass from the structures causing the gravity high in the first segment do not influence the gravity field and no gravity high is observed.

The results of the curvature analysis show that the calculated field was better reproduced in the preferred model than in the alternative version in which the gravity high of the southern Bahía Mansa-Osorno segment at the Longitudinal Valley was modelled using a dense and a thick crust. Therefore, it is postulated that, based on the gravity data, the Bouguer anomaly high associated with the Longitudinal Valley is better produced by a shallow mantle than by a dense and thick crust.